JGR Earth Surface

RESEARCH ARTICLE
10.1029/2021JF006194

Simulated Dynamics of Mixed Versus Uniform Grain Size Sediment Pulses in a Gravel-Bedded River

Muneer Ahammad[1], Jonathan A. Czuba[1], Allison M. Pfeiffer[2], Brendan P. Murphy[3], and Patrick Belmont[4]

[1]Department of Biological Systems Engineering, Virginia Tech, Blacksburg, VA, USA, [2]Department of Geology, Western Washington University, Bellingham, WA, USA, [3]School of Environmental Science, Simon Fraser University, Burnaby, BC, Canada, [4]Department of Watershed Sciences, Utah State University, Logan, UT, USA

Key Points:

- Channel incision may occur instead of aggradation when pulse volume is relatively small and pulse grain size is finer than bed
- Intermediate grain size pulses have the largest downstream effects; finer sizes translate quickly and coarser sizes disperse slowly
- A mixed-distribution pulse with smaller median grain size than the bed increases bed mobility more than a uniform-distribution pulse

Supporting Information:

Supporting Information may be found in the online version of this article.

Correspondence to:

J. A. Czuba,
jczuba@vt.edu

Citation:

Ahammad, M., Czuba, J. A., Pfeiffer, A. M., Murphy, B. P., & Belmont, P. (2021). Simulated dynamics of mixed versus uniform grain size sediment pulses in a gravel-bedded river. *Journal of Geophysical Research: Earth Surface*, *126*, e2021JF006194. https://doi.org/10.1029/2021JF006194

Received 1 APR 2021
Accepted 26 SEP 2021

Abstract Mountain rivers often receive sediment in the form of episodic, discrete pulses from a variety of natural and anthropogenic processes. Once emplaced in the river, the movement of this sediment depends on flow, grain size distribution, and channel and network geometry. Here, we simulate downstream bed elevation changes that result from discrete inputs of sediment (~10,000 m^3), differing in volume and grain size distribution, under medium and high flow conditions. We specifically focus on comparing bed responses between mixed and uniform grain size sediment pulses. This work builds on a Lagrangian, bed-material sediment transport model and applies it to a 27 km reach of the mainstem Nisqually River, Washington, USA. We compare observed bed elevation change and accumulation rates in a downstream lake to simulation results. Then we investigate the magnitude, timing, and persistence of downstream changes due to the introduction of synthetic sediment pulses by comparing the results against a baseline condition (without pulse). Our findings suggest that bed response is primarily influenced by the sediment-pulse grain size and distribution. Intermediate mixed-size pulses (~50% of the median bed gravel size) are likely to have the largest downstream impact because finer sizes translate quickly and coarser sizes (median bed gravel size and larger) disperse slowly. Furthermore, a mixed-size pulse, with a smaller median grain size than the bed, increases bed mobility more than a uniform-size pulse. This work has important implications for river management, as it allows us to better understand fluvial geomorphic responses to variations in sediment supply.

Plain Language Summary Sediment often enters mountain rivers from a variety of natural and human sources. Here, we simulate how this added sediment results in downstream changes in the amount of sediment in the river channel. This work was applied to a 27 km section of the Nisqually River, Washington, USA. We compare observed changes in the level of the stream bottom and accumulation rates in a downstream lake to model results. Then we investigate the magnitude, timing, and persistence of downstream changes due to the introduction of added sediment by comparing the changes against a baseline condition (without the added sediment). We found that added sediment particles that are half as large as on the riverbed and with a range of sizes are likely to have the largest downstream impact because smaller sizes move quickly and larger sizes move slowly. Furthermore, added sediment particles that are smaller than on the riverbed and with a range of sizes help more sediment particles on the riverbed move than if that sediment addition all had the same particle size. This work has important implications for river management, as it allows us to better understand how rivers are affected by variations in added sediment.

1. Introduction

Sediments are delivered into river networks from the surrounding watershed, often as discrete pulses in space and time driven by precipitation or other perturbations (Benda & Dunne, 1997b; Gran & Czuba, 2017; Murphy et al., 2019). This stochastic supply of sediment may enter the river network from a variety of watershed sources such as uplands, ravines, banks, bluffs, landslides, and debris flows (Benda & Dunne, 1997b; Czuba et al., 2017; Murphy et al., 2019). In mountain streams, coarse sediment pulses are commonly supplied in large volumes from episodic mass movements like landslides and debris flows (Benda & Dunne, 1997b; Cui, Parker, Lisle, et al., 2003; Cui, Parker, Pizzuto, & Lisle, 2003). Wildfire is a major effect of climate change and post-wildfire landscapes can deliver large quantities of sediment to streams

(Benda et al., 2004; Moody & Martin, 2004; Murphy et al., 2018, 2019; Sankey et al., 2017). Anthropogenic perturbations can also alter the frequency and magnitude of sediment supply, such as through dam removal (Cashman et al., 2021; Czuba et al., 2011; Dow et al., 2020; East et al., 2015, 2018; Major et al., 2012; Ritchie et al., 2018) and gravel augmentation (Arnaud et al., 2017; Gaeuman et al., 2017; Welber et al., 2020). Once delivered into a river, a pulse of sediment moves downstream through some combination of translation, dispersion, and attrition of particles (An et al., 2017; Cashman et al., 2021; Cui & Parker, 2005; Cui, Parker, Lisle, et al., 2003; Cui, Parker, Pizzuto, et al., 2003; East et al., 2015, 2018; Lisle, 2008; Lisle et al., 1997, 2001; Major et al., 2012; Ritchie et al., 2018; Sklar et al., 2009; Sutherland et al., 2002) or can be stored within the river and floodplain network (Benda & Dunne, 1997a; Cashman et al., 2021; Gran & Czuba, 2017).

When a sediment pulse is emplaced on the bed, the river adjusts to process the additional sediment (Cui, Parker, Lisle, et al., 2003). The evolution of sediment pulses is influenced by river channel morphology and bed texture (Lisle, 2008), river network structure (Gran & Czuba, 2017), and watershed historical legacy (James, 2010). In gravel-bed rivers, sediment pulses evolve by translation when pulses are composed of fine-grained sediment, specifically finer than the underlying bed material, and when pulses have narrow grain size distributions with small volumes (Cui & Parker, 2005; Cui, Parker, Lisle, et al., 2003; Cui, Parker, Pizzuto, & Lisle, 2003; Lisle, 2008; Lisle et al., 1997, 2001; Sklar et al., 2009). In contrast, dispersion of sediment pulses occurs when the pulse has a wide grain size distribution, sediment coarser than the preexisting bed, or a large volume relative to channel dimensions, or where the Froude number of the flow is high (>0.4) and conditions of the river promote differential transport of sediment (Cui & Parker, 2005; Cui, Parker, Lisle, et al., 2003; Cui, Parker, Pizzuto, et al., 2003; East et al., 2015; Lisle, 2008; Lisle et al., 1997, 2001; Sklar et al., 2009). At large spatial scales, the sediment pulse grain size distribution may fine downstream due to size-selective transport or attrition, especially when transport distances are long or particles are friable (Ashworth & Ferguson, 1989; Dingle et al., 2017; O'Connor et al., 2014; Paola et al., 1992; Parker, 1991). The gradual downstream progression of sediment pulse movement may be interrupted by sediment bottlenecks, which are locations in river networks with local deceases in transport capacity due to low channel slopes and/or wide channel widths (Czuba et al., 2017; Gran & Czuba, 2017; Schmitt et al., 2018).

The evolution of a sediment pulse is also dictated by pulse characteristics, streamflow hydrology, and channel properties (Cui & Parker, 2005; Czuba, Magirl, et al., 2012; Murphy et al., 2019; Sklar et al., 2009). River reaches with high slope or discharge relative to the bed surface grain size, i.e., high bedload transport capacity, can move sediment pulses quickly while reaches with low sediment-transport capacity and stream power are prone to sedimentation (Cui & Parker, 2005; Czuba, Magirl, et al., 2012; Murphy et al., 2019). Bed texture response to a sediment pulse also depends on the grain size of the pre-existing bed, pulse size, pulse volume, and the spatial and temporal evolution of the pulse (Sklar et al., 2009). Sediment pulses with a grain size smaller than the preexisting bed move rapidly and thus, lead to a greater decrease in median bed material size, but for a shorter duration compared to a coarser sediment pulse undergoing more dispersion (Sklar et al., 2009). Large pulse volumes create longer-lasting impacts on the channel bed with more dispersion compared to small-volume pulses (Czuba, Magirl, et al., 2012; Murphy et al., 2019; Sklar et al., 2009). Sediment pulses are moved downstream more rapidly as the magnitude or frequency of streamflow increases (Czuba, Magirl, et al., 2012). Thus, the interplay among sediment pulse characteristics of grain size, grain size distribution, and volume along with channel and flow properties determine how the pulse evolves through a river network.

Along with flume experiments and model simulations with simple geometry, recent field studies describe how sediment pulses, particularly following dam removal, evolve over long reaches in actual rivers with downstream variations in bed sediment grain size, slope, and width (Cashman et al., 2021; East et al., 2018, 2015; Harrison et al., 2018; Major et al., 2012; Pace et al., 2017; Ritchie et al., 2018; Warrick et al., 2015). Following the removal of Simkins Dam on the Patapsco River in Maryland, Cashman et al. (2021) found weeks to months of translation and dispersion of the sediment pulse within the channel, which aggraded the bed and affected local hydraulics. Dispersion and deposition on floodplains persisted for years. Following the removal of two dams on the Elwha River in Washington, approximately 65% of the reservoir sediment was eroded, with 10% of this eroded sediment aggrading the channel up to 1 m in places (deeper in pools), and channel morphology changed from pool-riffle to braided (East et al., 2015, 2018; Ritchie et al., 2018; Warrick et al., 2015). Furthermore, the most change occurred within the first two years

following the dam removals (without any large flows) over the 20 km reach from the upstream-most dam to the coast. Following the removal of Marmot Dam on the Sandy River in Oregon, Major et al. (2012) found that sediment transport and deposition were strongly controlled by downstream changes in channel slope and valley morphology. Thus, variable transport capacity conditions present in the field strongly influence sediment pulse behavior. Such variability is rarely represented in network scale sediment routing models, which presents a potentially large gap in our ability to predict how such pulses may evolve during transport downstream through real river networks.

It is difficult to capture all the complex processes of sediment transport across a large-scale in a single modeling framework. There are one-dimensional models available that can be utilized to simulate sediment-pulse dynamics. The Unified Gravel-Sand (TUGS) model uses a surface-based bedload equation, with a sand and gravel transfer function, in linking grain size distribution in the bed load, surface, and subsurface layer to simulate transport, erosion, and deposition of sand and gravel (Cui, 2007). Specifically applied to dam removal pulses, the Dam Removal Express Assessment Models (DREAMs) simulate aggradation and incision following dam removal for reservoir deposits composed primarily of noncohesive sand and silt (DREAM-1) and gravel (DREAM-2; Cui et al., 2006a, 2006b). The Morphodynamics and Sediment Tracers in one-dimension (MAST-1D) model also incorporate particle-size distributions to simulate morphodynamic evolution of a river bed and lateral exchange of sediment between the channel and floodplain (Lauer et al., 2016; Viparelli et al., 2013). The Lagrangian framework presented by Czuba (2018) and Pfeiffer et al. (2020) also uses a surface-based bedload equation and considers mixed-size sediment transport. This model can be applied in gravel-bedded river networks as it is capable of incorporating additional complexities that arise from channel network structure. While these 1D models represent a promising avenue for the study of sediment pulse dynamics, to date there are few examples of model application with field data over spatial scales of many kilometers (Castro-Bolinaga et al., 2020; Cui et al., 2014, 2019; De Rego et al., 2020).

We investigate the space-time evolution and downstream effects of simulated sediment pulses in the mainstem Nisqually River in Washington, USA. We simulate pulse behavior with downstream variations in slope, width, and bed-sediment grain size using a Lagrangian, bed-material sediment transport model (Czuba, 2018). Using this model, we explore how mixed-size sediment pulses, which are common in the field, affect downstream bed elevations, grain size, and sediment transport differently than uniform-sized sediment pulses, which have been commonly studied (as described above). We focus on sediment pulse volumes on the order of 10,000 m^3, typical of small dam removals and gravel augmentation (Arnaud et al., 2017; Bellmore et al., 2017; Foley et al., 2017; Major et al., 2017), which would be commonly encountered by river managers. Results of model simulations were compared to physical measurements, where available, to assess the efficacy of the model in predicting sediment transport and resulting changes. While we discuss limitations of our model in representing all the relevant complexities of the Nisqually River, we suggest that the model adequately represents an example gravel-bedded river, constrained in reality, and offers insight into how sediment pulses might move through real river systems. This study adds to our collective knowledge of how sediment supply perturbations, as discrete sediment pulses, may evolve in rivers and impact downstream locations.

2. Study Area

Mount Rainier is a glaciated stratovolcano in the Cascade Range of western Washington with a summit elevation of approximately 4,393 m. The Nisqually River drains the southwestern slope of Mount Rainier and terminates in Puget Sound. This river system, and also the White, Carbon, and Puyallup Rivers that drain Mount Rainier, receives large sediment loads during large floods along with substantial debris flows (e.g., 40 million m^3 during a rainfall event in 1947) from Mount Rainier (Anderson & Pitlick, 2014; Czuba, Magirl, et al., 2012; Legg et al., 2014). Large sediment loads delivered to these rivers contribute to river channel migration, bed aggradation, and subsequent reduction of flood-conveyance capacity (Czuba et al., 2010). The Nisqually River drains approximately 2,000 km^2, but Alder Lake divides the river into upper and lower sections. Alder Lake is a reservoir, created behind Alder Dam in 1945, which reduces downstream sediment delivery (Czuba, Olsen, et al., 2012). Herein, we focus on the upper Nisqually River draining Mount Rainier, which is most affected by large sediment supply. The upper Nisqually River (referred to as the Nisqually River hereafter) drains approximately 590 km^2 upstream of Alder Lake (Figure 1). Forest is the dominant

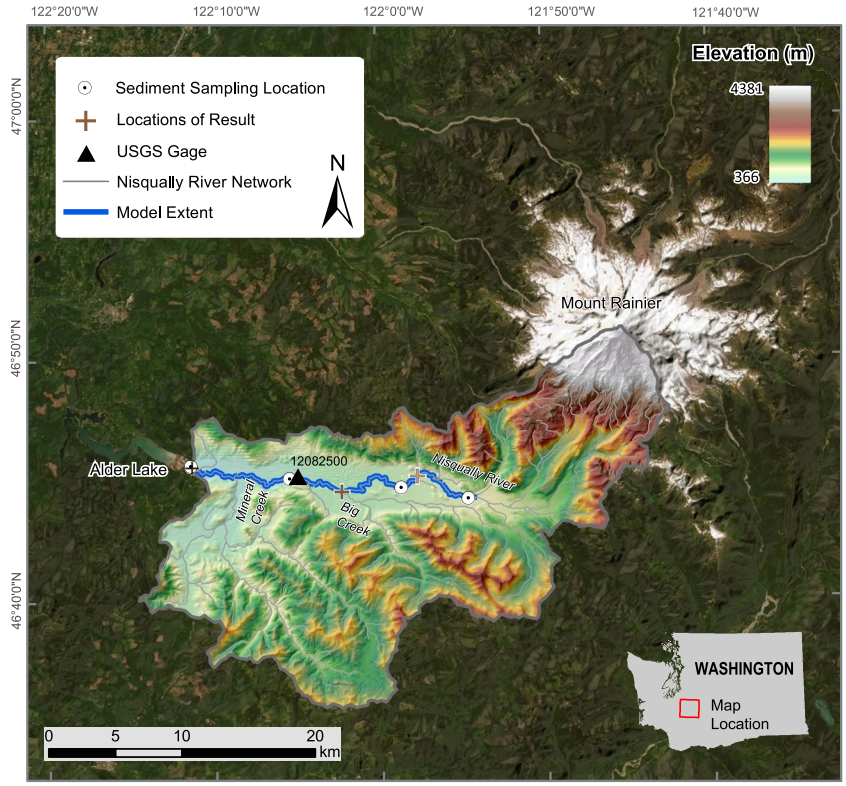

Figure 1. Study area map of the Nisqually River, Washington, USA. The USGS gage (black triangle) and locations of simulation results (brown plus signs) are marked within the modeled reach along with bed material sediment sampling locations (white circles).

land cover here and some upstream tributaries drain active glaciers. We apply our model here, because this is a reach commonly affected by large sediment pulse inputs and data are available to develop a model and assess the results (further described below).

3. Methods

3.1. Model Framework and Development

3.1.1. Two-Layer River-Network Model

This work builds on a previous 1D Lagrangian, bed-material sediment transport model (Czuba, 2018), which we briefly summarize in this section. Here, sediment is conceptualized as a set of discrete individual parcels, where each parcel has a volume and grain size. The river network is conceptualized as interconnected links, each with topologic (downstream connectivity), geometric (elevation, slope, channel segment length, average width), hydrodynamic (flow discharge), and bed sediment attributes (grain size distribution). Sediment in any link at any time is separated into two layers: active surface layer and inactive subsurface layer.

The maximum volume of sediment (χ) that can be moved in any link at any time is set by:

$$\chi = \ell B L_a \tag{1}$$

where ℓ is the link length, B is the channel width, and L_a is the active layer thickness of that link. The total sediment parcel volume in any link at any time (V) is the sum of the volumes of all parcels within that link at that particular time. If the total sediment parcel volume in a link exceeds χ, then the excess sediment parcels are inactivated and placed into the subsurface layer, which consequently increases the slope of that link and decreases the slopes of any upstream links (Czuba et al., 2017).

The total sediment volume in the active surface layer of any link at any time (V_{act}) is dependent on χ as:

$$V_{act} = \begin{cases} V, & V < \chi \\ \chi, & V \geq \chi \end{cases} \quad (2)$$

Each sediment parcel is tracked as it moves through the network. The arrival and departure of parcels from links follow a first-in, last-out rule, i.e., the most recent parcels to arrive in a link are positioned in the active surface layer, whereas the oldest parcels in the link would be selected first for inactivation in the subsurface layer as described above. With this movement of sediment, bed elevation, and thereby slope, is updated accordingly (accounting for porosity) at each time step throughout the network. The transport time (t) of a sediment parcel to move through link length ℓ (Czuba, 2018; Czuba & Foufoula-Georgiou, 2014) is calculated as:

$$t = \frac{\rho^{3/2} g R \ell L_a}{W^* \tau^{3/2} F} \quad (3)$$

where ρ is the density of water, g is the acceleration due to gravity, R is the submerged specific gravity of sediment, W^* is a dimensionless transport rate, τ is the bed shear stress, and F is a fraction describing the ratio of the parcel volume to the total sediment volume in the active surface layer, V_{act}, of that link at that time. The dimensionless transport rate, W^*, is calculated for each parcel and comes from the surface-based, mixed-size bedload transport equation of Wilcock and Crowe (2003). This formulation was chosen because it takes into consideration that the presence of sand increases the mobility of sediment.

The model requires flow data, channel/link data (segment length, width, initial elevation), and initial sediment data as inputs. The simulation procedure for every link at each time step can be summarized as:

1. compute the maximum volume of sediment χ that can be moved (Equation 1),
2. compute bed elevations from sediment volume and update slope,
3. compute grain size information of the active layer from all sediment parcels in the active layer for the Wilcock and Crowe (2003) equation,
4. compute transport time of each parcel (Equation 3), and,
5. update all parcel locations in their current link or move to a downstream link.

Thus, model outputs include spatially and temporally explicit characterization of sediment depth (accounting for porosity), bed elevation, grain size distribution, and volume in any link of the river network including fluxes past the downstream outlet. The Lagrangian nature of this formulation also allows specific sediment inputs to be tracked as they move through the river network.

3.1.2. Key Modeling Advancements

3.1.2.1. Initial Median Sediment Size

The Nisqually River is gravel-bedded, and we are representing it as a single-thread channel whose median bed particle size varies systematically with local hydraulics. Specifically, the initial median bed particle size (D_{50}) was initialized throughout the network as a function of channel width (B) and slope (S) following a reduced form of the equation provided by Snyder et al. (2013) as:

$$D_{50} = \frac{n^{3/5} Q_2^{3/5} S^{7/10}}{R \tau_c^* B^{3/5}} \quad (4)$$

where n is the Manning roughness coefficient, Q_2 is the 2-year recurrence interval flow, and τ_c^* is the critical Shields parameter to mobilize D_{50}. We implement Equation 4 using an assumed τ_c^* of 0.04 and n of 0.035, as in Snyder et al. (2013). Rather than validating these particular parameter values, we simply validate the resulting estimates of D_{50} with field measurements at several points along the study reach.

3.1.2.2. Flow Depth

We consider river flows as hydraulically rough flows. Using the depth-average velocity, water depth in each link in the model is calculated as:

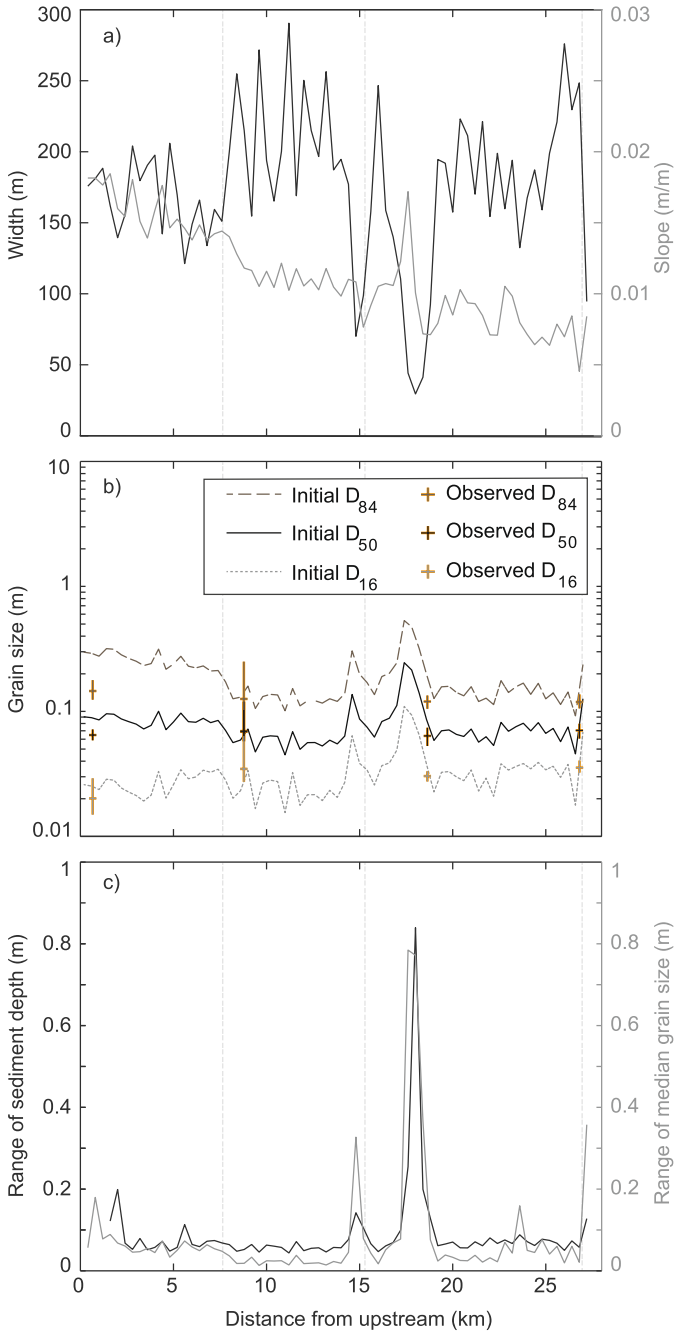

Figure 2. Fluvial geomorphic attributes along the mainstem Nisqually River. (a) Width and initial bed slope of the Nisqually River. (b) Observed (plus sign, where the vertical line of the plus represents the range) and modeled (solid and dashed lines) initial bed surface material grain size (excluding sand) from Equation 4. The observed D_{50} at roughly 9 km distance from upstream has a thicker symbol than the other observed grain sizes to show the extents of overlapping vertical lines. (c) Simulated range of sediment depth and median grain size (excluding sand) from 1946 to 2011. The three-light gray vertical lines represent the locations where results are shown in Figures 3b and 3c.

$$H = \left(\frac{Qk_s^{1/6}}{8.1B\sqrt{gS}} \right)^{3/5} \quad (5)$$

where k_s is an effective roughness height (later assigned as a function of bed grain size in Section 3.2). This relation is approximated from Keulegan's resistance law for rough flow (Garcia, 2008; Keulegan, 1938) to incorporate grain-induced resistance in gravel-bed rivers. The formulation of Equation 5 allows water depth to change with variations in discharge (Q) and channel flow resistance (via k_s).

3.1.2.3. Upstream Background Sediment Supply

Sediment can be supplied anywhere along any link within the network at any time step. We considered several different methods for supplying upstream background sediment to the model, each of which is described in Supporting Information S1. The method that was the most numerically stable for this application and used throughout this study involved creating a sediment supply reservoir at the upstream end of the model. We did this by adding sediment parcels to the bed surface layer at the most upstream link in a sufficient volume as to not empty during the simulation. We also fixed the bed elevation at the upstream end of this link so that the added bed volume did not increase the channel slope. The streamflow continuously eroded this background sediment from this sediment supply link and transported it downstream.

3.2. Model Parameterization

This study modeled a 27.2 km reach of the mainstem Nisqually River discretized into 400 m long links, which is roughly twice the channel width, starting at Tahoma Creek (beginning of model stationing) and ending at Alder Lake (68 links total; Figure 1). We used the input channel geometry, streamflow, and sediment data from the model used by Czuba, Magirl, et al. (2012). The channel geometry data included channel widths and bed elevations. The active channel, defined as the section of the river corridor relatively free of vegetation that conveys the majority of the water and sediment during high flow, was digitized from the 2009 National Agricultural Imagery Program imagery at 1:3,000 scale (U.S. Department of Agriculture, 2011). A river centerline was then digitized through the center of the active channel, representing the dominant pathway of the river during high flow. Major tributaries include Big and Mineral Creeks (Figure 1). The active-channel width (Figure 2a) for each 400 m link was computed by dividing the total active-channel area for 400 m segments of the channel centerline by the length of that segment (400 m).

A longitudinal profile approximating the water-surface elevation was obtained by extracting lidar elevations of the river centerline. Elevation points were sampled from the underlying 1 m bare-Earth lidar data (PSLC, 2012) at 10 m increments along the river centerlines and averaged together every 400 m to determine an average elevation for that link. The final linear network in the model started just downstream of the confluence of the Nisqually River and Tahoma Creek, where the bed slope was roughly 2% (Figure 2a). A minimum slope of 0.1% was imposed for all links to account for any erroneously low-sloped sampling points.

A long-term streamflow record (water years 1946–2011) was compiled using time series of daily streamflow (Figure 3a) from a USGS streamflow-gaging station (see location in Figure 1) on the Nisqually River (USGS

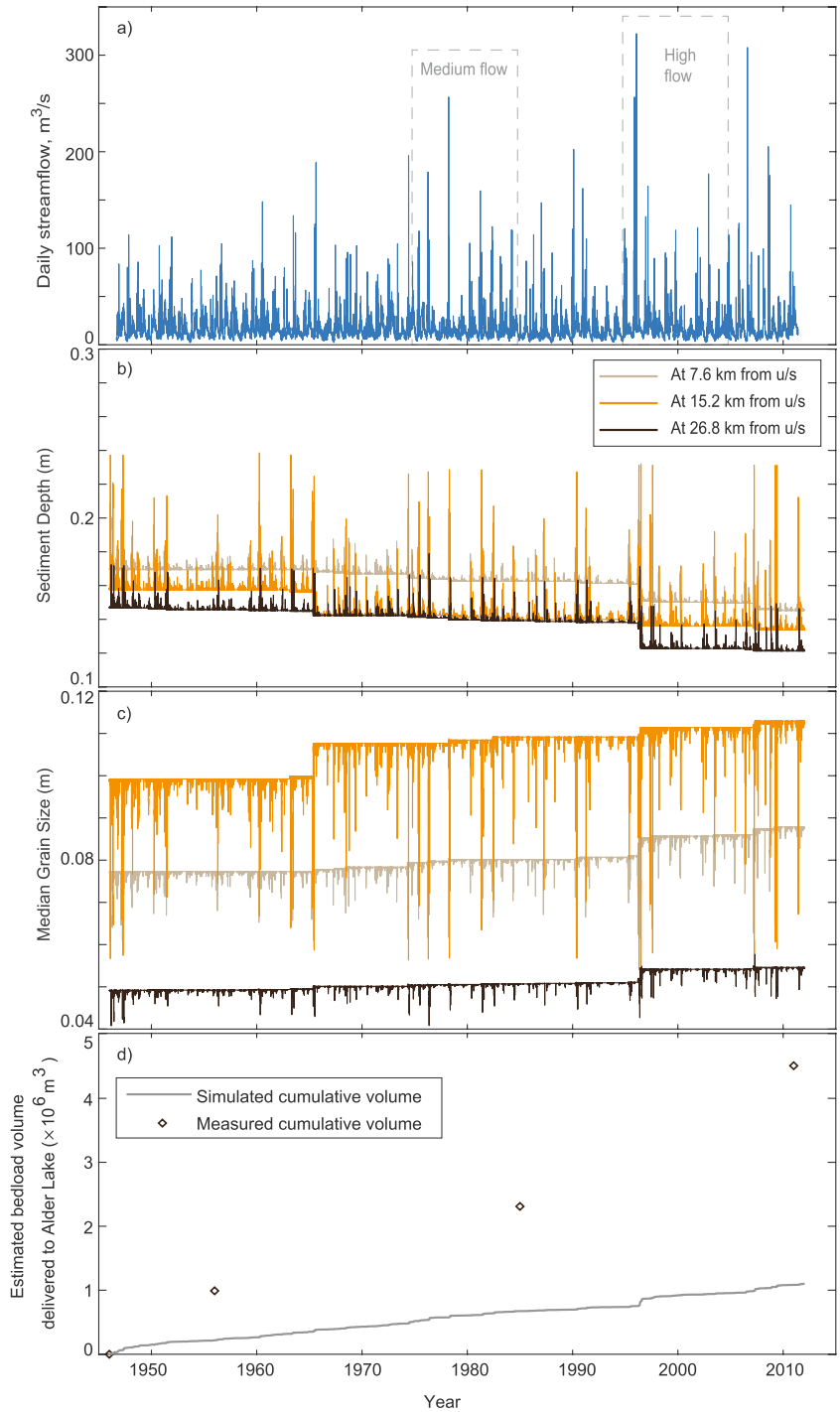

Figure 3. Time series of flow and sediment characteristics at three links and the outlet. (a) Daily streamflow at the upstream end of the model. The high flow and medium flow periods (discussed in Section 3.4) are shown in dashed rectangles. (b) Sediment depth and (c) median grain size in three links located in Figure 1 (brown plus signs). (d) Estimated (simulated and measured) bedload contribution to Alder Lake from 1946 to 2011.

12082500, Nisqually River near National, WA; USGS, 2021). The streamflow data measured at this gage was scaled to upstream and downstream flow-change locations (Big and Mineral Creeks; Figure 1) using contributing drainage area. From the upstream end of the model to Big Creek (at 14.6 km), the gage discharge was decreased by 30%, and from Mineral Creek (at 23.6 km) to the downstream end of the model, the gage discharge was increased by 60%.

All sediment parcels were assigned a maximum parcel volume of 50 m^3. Grain size of any parcel was given a discrete value among 0.4, 2.83, 5.66, 16.0, 45.3, 90.5, 181, 362, 724.1, and 1,448.2 mm, which are the mean sizes for sand and of gravel (computed in log scale) within grain size bins bounded by 2, 4, 8, 32, 64, 128, 256, 512, 1,024, and 2,048 mm. There were four surface grain size sampling locations (Figure 1; Czuba, Magirl, et al., 2012), and multiple measurements were taken from gravel bars at each site using the Wolman pebble-count method (Wolman, 1954). These distributions had a median gravel size of roughly 70 mm and were composed of roughly 40% sand. The initial gravel distribution was approximated as log-normal with gravel sizes for each link calculated from Equation 4 (with Manning's n as 0.035 and τ_c^*as 0.04; Snyder et al., 2013) and standard deviation calculated from the observed distributions ($\sqrt{D_{84}/D_{16}} \sim$ 2–3 mm, Figure 2b; Garcia, 2008). This served as a close starting point for setting the initial bed sediment distribution that was further modified during a model conditioning run. In Figure 2b, the observed field measurements are shown as plus marks, the vertical lines of which extend to the range of the gravel size measurements and horizontal lines of the plus signs represent the median observed gravel size at that location. Due to the absence of subsurface data, it was initialized to be the same as the surface size distribution. Sediment load by grain size, was supplied to the model at the upstream boundary, and the determination of which was discussed in Section 3.1.2.3.

The roughness height k_s (Equation 5) was assumed here as twice the median particle size (Garcia, 2008) and was updated at each time step in the model to translate flow discharge to flow depth. The active surface-layer thickness was selected as 0.25 m (close to D_{90}) throughout the model and bed sediment porosity was set as 0.25. Other specific parameter values were $\rho = 1{,}000$ kg/m^3, $g = 9.81$ m/s^2, and $R = 1.65$.

The model was first run from October 1, 1945 to September 30, 2011 (water years 1946–2011) for conditioning of input data. The model-conditioning process is a 1D river-morphodynamic adjustment process, which allows free or unconstrained parameters (e.g., bed sediment grain size distribution) to adjust to the fixed or constraining parameters in a way that allows the model to better simulate river processes given sparse topographic and sediment data (Cui & Wilcox, 2008; Cui et al., 2006a, 2006b; Lauer & Parker, 2008). The entire 65-year streamflow record was simulated and the model reached quasi-equilibrium after around 35 years, when the model simulated short-term fluctuations in bed elevation (mainly with flow fluctuations), but minimal long-term change. At the end of the model-conditioning process, the conditioned bed sediment grain size distribution was used at the start of all subsequent model simulations. Thus, only the bed sediment size distribution was updated while other inputs (e.g., slope, bed elevation etc.) were not updated following the model-conditioning process.

3.3. Model Verification

After model conditioning, the model was run again using daily streamflow data from water years 1946–2011. The simulated sediment depth and median grain size at three different locations are shown in Figures 3b and 3c. These locations are marked in Figure 1 (as brown plus signs): at an upstream location (7.6 km), in the middle of the reach (15.2 km), and at a downstream location near the basin outlet (26.8 km). The solid line in Figure 3d shows simulated bedload volume to Alder Lake. Changes in sediment depth, grain size, and volume were the greatest during high flows. The gradual decrease in equilibrium sediment depth (~3 cm over 65 years) in the baseline scenario simulated by the model suggests minor incisions would occur during high flows given the minimal baseline sediment supply simulated. Gradual coarsening of the median grain size suggests that this transport is mainly winnowing fine material. The model was only able to maintain a bed material composition at or below approximately 5% sand (much lower than the observed 40% on gravel bars). During the conditioning run, the model became stable when the bed material sand in excess of 5% was transported out of the model domain. The gravel bars from which the bed material was measured were very sandy, yet there was considerably less sand in the low-flow channel beds. We believe

some of this discrepancy between our field observations and simulated sand fractions has to do with sorting and winnowing that occurs in the more complex field channel geometry than we are capturing in our essentially 1D model. We discuss this issue further in Section 5.3 along with steps for potential model improvement. The abrupt changes in bed elevation during high flow events correspond to abrupt increases in simulated outlet volume. Figure 3c shows coarser bed material in the middle link compared to upstream and downstream locations, which is due to the initially coarser material at that location (middle light gray vertical line in Figure 2b). Results demonstrate relatively stable sediment characteristics with short-lived high flow fluctuations, while long-term trends in grain size and sediment depth were gradually adjusted primarily during high flow events.

We compared the model results to available measurements of bed grain size data, gage height fluctuations (at USGS 12082500, Nisqually River near National, WA), and deposition records in Alder Lake. We observed from Figure 2b that initial median gravel sizes (from Equation 4) exhibit strong agreement with median sizes of that collected at four locations in the network. Thus, this approach (via Snyder et al., 2013) allowed us to vary initial sediment size throughout the network as a function of channel geometry. The observed variance in bed elevations at the USGS gage location (at around 18 km) was ~1.5 m during 1985–2011 (Czuba, Magirl, et al., 2012; Pfeiffer et al., 2019). The model predicted that bed elevations varied 0.9 m (peak of sediment depth in Figure 2c) from equilibrium during this same period. However, this was under a simulated background sediment supply that was transporting at-capacity, thus, not including sediment pulses that likely contributed to real variations observed in the gage data (Anderson & Pitlick, 2014; Legg et al., 2014). There were 48 debris-flow events recorded between 1926 and 2006 in tributaries of the Nisqually River within Mount Rainier, 28 of which occurred between 1967 and 2006 (Copeland, 2009; Walder & Driedger, 1993, 1994). We also know that a heavy rainfall event in 1947 alone delivered about 40 million cubic meters of sediment to a Nisqually River tributary (Crandell, 1971).

Estimating bedload transport only, the model underpredicted the delta volume in Alder Lake (Czuba, Olsen, et al., 2012) by approximately four-fold (Figure 3d). In the White River (a comparable river draining Mount Rainier), the bedload contribution to the total load was low (around 11%; Czuba, Magirl, et al., 2012), and most of the material in transport was in suspension (Czuba, Magirl, et al., 2012). We used this percentage (11%) to convert the total volume of sediment accumulated in Alder Lake to an estimated fraction that was delivered by bedload (Figure 3d). We did not include fine suspended material in our simulation and could not adequately simulate the total amount of sand transported in this system. Given potential changes in delta depositional porosity and incomplete sediment input records (e.g., 48 debris-flow events not included), we fully expect our simulations to underestimate both bed elevation changes and outlet volumes. For instance, even if only a small fraction of the 40 million cubic meters of sediment deposited in a Nisqually River tributary from a single debris flow event in 1947 (Crandell, 1971) eroded over time to deliver three million cubic meters of sediment to Alder Lake as bedload, this would make up for the underestimation in the model simulation. Altogether, these factors likely contributed to the low predictions of bed elevation fluctuations and volume delivered to Alder Lake as compared to observations of deposition in the delta of Alder Lake. However, we do think the model adequately represents an example gravel-bedded river, constrained in reality, and should offer insight into how sediment pulses might move through real river systems.

3.4. Model Simulations and Analysis Metrics

Model simulations investigated the spatial and temporal evolution and downstream effect of uniform-sized and mixed sediment pulses in a river with downstream variations in slope, width, and bed-sediment grain size. Model simulations included combinations of two hydrologic conditions, two sediment-pulse volumes, two sediment-pulse distribution types, and three sediment-pulse grain sizes. We constructed seven comparative analyses (See Table 1 in Section 4.1), from which three comparisons between uniform-sized and mixed sediment pulses are detailed in Section 4.2 (others are in Supporting Information S1). The set of model simulations varied hydrologic conditions (repeating 10-year periods for 30 years of daily streamflow for high (WY 1995–2004; highest two peak flows = 322 m^3/s and 257 m^3/s) and medium (WY 1975–1984; highest two peak flows = 257 m^3/s and 179 m^3/s) streamflow hydrology; see Figure 3a), sediment-pulse volume (reported as a depth; 0.4 and 1.1 m supplied to the upstream-most link of the network), sediment-pulse

Table 1
Summary of the Comparisons of Model Simulation Results

Difference in:	Flow	Pulse depth (m)	Median pulse grain size (mm)	Highlight
Median gravel size of pulse	Medium	0.4	10	Finer pulse travels faster and causes more incision, while coarser pulse travels slower and causes more aggradation (especially at wider reaches with low slope)[a]
	Medium	0.4	30	
	High	0.4	30	Coarse pulse travels slower and leaves greater post-pulse incision. Complex pattern of bed-elevation change at intersection of pulse size, channel characteristics, and hydrology[a]
	High	0.4	70	
Pulse volume (Depth)	Medium	0.4	30	Nearly similar bed-elevation change for both pulse depths. Smaller volume took longer to move through system, likely due to more fully mixing with the bed material[a]
	Medium	1.1	30	
Flow	Medium	0.4	30	Pulse travels faster during high flow. Pattern of bed-elevation change highly variable[a]
	High	0.4	30	
Pulse distribution type	Medium	0.4	10	Arrival time of 50% of pulse is the same, but coarse tail of mixed pulse moves slower. Bed-elevation change (primarily incision) is greater for the uniform pulse (Section 4.2.1)
	Medium	0.4	10 (Mixed)	
	Medium	0.4	30	Arrival time of 50% of pulse is the same, but coarse tail of mixed pulse moves slower. Pattern of bed-elevation change highly variable. (Section 4.2.2)
	Medium	0.4	30 (Mixed)	
	Medium	1.1	70	Mixed pulse dispersed slowly without a defined pulse manifestation. (Section 4.2.3)
	Medium	1.1	70 (Mixed)	

[a]Findings can be found in Supporting Information S1.

distribution type (uniform-sized gravel and mixed distribution), and sediment-pulse median grain size (10, 30, and 70 mm; recall that the median gravel size of the bed was approximately 70 mm, so these pulse grain sizes are roughly 0.15, 0.5, and 1.0 times the median bed gravel size). Sediment-pulse depths (0.4 and 1.1 m) were converted from sediment-pulse volumes (of roughly 19,000 and 57,000 m^3, respectively) by dividing by the average link length and width, and accounting for porosity. That is, if the pulses of above-mentioned volumes were emplaced in a single link of average width, these pulses would aggrade the bed (or increase the sediment depth) by 0.4 and 1.1 m, respectively. Thus, sediment-pulse depths represent pulses of different sediment volumes. These pulse volumes are roughly one and three times, respectively, the transport capacity volumes, χ, of the most upstream link. Additionally, these pulse volumes are representative of inputs from most dam removals (94% of removed dams impounded less than 10,000 m^3 of sediment; Bellmore et al., 2017; Foley et al., 2017; Major et al., 2017) and also from gravel augmentation (23,000 m^3 of sediment; Arnaud et al., 2017). The mixed-type sediment distribution was constructed assuming a log-normal sediment distribution with the specified median gravel size and standard deviation from field measurements, and then incorporating 5% sand fraction (estimated from the conditioning run). For each hydrologic condition, the simulation results of a baseline condition (without a sediment pulse) were subtracted from a sediment-pulse condition (with different pulse volumes, distribution types, and grain sizes) to isolate the morphodynamic response due to the individual sediment pulse. Each sediment pulse was added in total, instantaneously to the model at the beginning of the model run (time $t = 0$) and at the second link from the upstream end (to avoid adding the pulse in the background sediment supply link).

The metrics we used to describe the downstream effect of a sediment pulse were the maximum change in bed elevation and median bed-surface gravel size, timing of maximum accumulation, and average change in post-pulse sediment depth. We compared the maximum changes and timing of maximum changes with different pulse arrival times. The arrival time of 50% of the pulse at a location is the time when half of a pulse's volume has been transported past that location. We were able to calculate this metric, because the

Lagrangian model used allows us to "tag" the pulse sediment parcels and know where they are located at any given time. Similarly, an arrival time of 10% and 90% of the pulse at a location are the times when one-tenth and nine-tenths of the pulse volume had transported past that location, respectively. The spread of timing, as defined for this study, is the difference in the arrival times of 90% and 10% of the sediment pulse by volume. If the simulated flows did not transport 90% of the pulse volume through a stated location (e.g., the outlet) by the end of the simulation, then the spread of timing was calculated by subtracting the pulse arrival time for the 10% volume from the duration of the simulation (i.e., 30 years). The average change in post-pulse sediment depth was calculated as the time-averaged change of sediment depth from the baseline condition after the peak bed-elevation change due to the pulse had passed each location. Normalized change in simulated outlet volume was found by dividing the change in outlet volume from the baseline condition by the input pulse volume.

4. Results

4.1. Overview of Pulse Dynamics and Movement

Nine sediment pulse runs were conducted to examine the impacts of median pulse grain size, volume (converted to a depth), and distribution type (uniform and mixed) along with two baseline runs (without pulse) under medium and high flow conditions. These simulations resulted in a total of seven comparisons, which are listed in Table 1. We also highlight the key findings of each comparison, the details of which are discussed in the following sections and in Supporting Information S1. We only present detailed comparisons between the uniform-sized and mixed pulses in the next section because these represent the most novel results. The other comparisons, which have been explored in previous literature, are detailed in Supporting Information S1.

Before describing the details of the runs and comparisons with differences in pulse distribution type, we provide an overview of simulated pulse movement as the fraction of the pulse that remains in the mainstem of the Nisqually River under different conditions (Figure 4). Compared with uniform pulses, mixed pulses moved more slowly through the system and were not completely delivered to the outlet by the end of the 30-year simulation (Figure 4; markers with an "×"). For example, under medium flow and for a 10 mm uniform pulse (filled green square marker), 100% of the pulse traveled through the network within the first 2 years. But for a mixed pulse with a D_{50} of 10 mm, only 70% of the pulse traveled through the network within 2 years and 83% of it reached the outlet within 30 years. For 70 mm pulses (orange square marker), the mixed pulse was transported slowly (71% reached the outlet after 30 years), whereas all of the uniform pulses traveled through the network within 14 years. For 30 mm pulses (filled blue square marker), 90% of the uniform pulse and 74% of the mixed pulse traveled through the network after 30 years. However, the larger volume uniform pulse (hollow blue square marker) traveled more rapidly than the smaller pulse volume of either uniform or mixed grains (filled blue square markers) under medium flows; the smaller volume pulse was likely mixing more with the bed material than larger volume pulses (discussed further in Text S3 in Supporting Information S1). High flows (filled blue circular markers) transported the pulse much quicker compared to medium flows – 97% within 2 years and 100% within 12 years. When high flows act on the system with a 90 mm pulse (filled orange circular markers), model simulations indicate 53% of the uniform pulse travels to the outlet within 2 years and 100% of it within 12 years. Thus, movement of sediment pulses through this reach depends on the dynamics of size, volume, distribution type, and flow condition, which we describe further in subsequent subsections and in Supporting Information S1.

4.2. Comparison of Changes From Different Pulse Grain Size Distributions

In this application, we systematically found that changes in median gravel size were inversely related to the changes in sediment depth (i.e., bed aggradation occurred with bed fining and bed incision occurred with bed coarsening; see Text S2 in Supporting Information S1). Thus, from here on, we narrow down our analysis to sediment depth only, in order to simplify the comparisons.

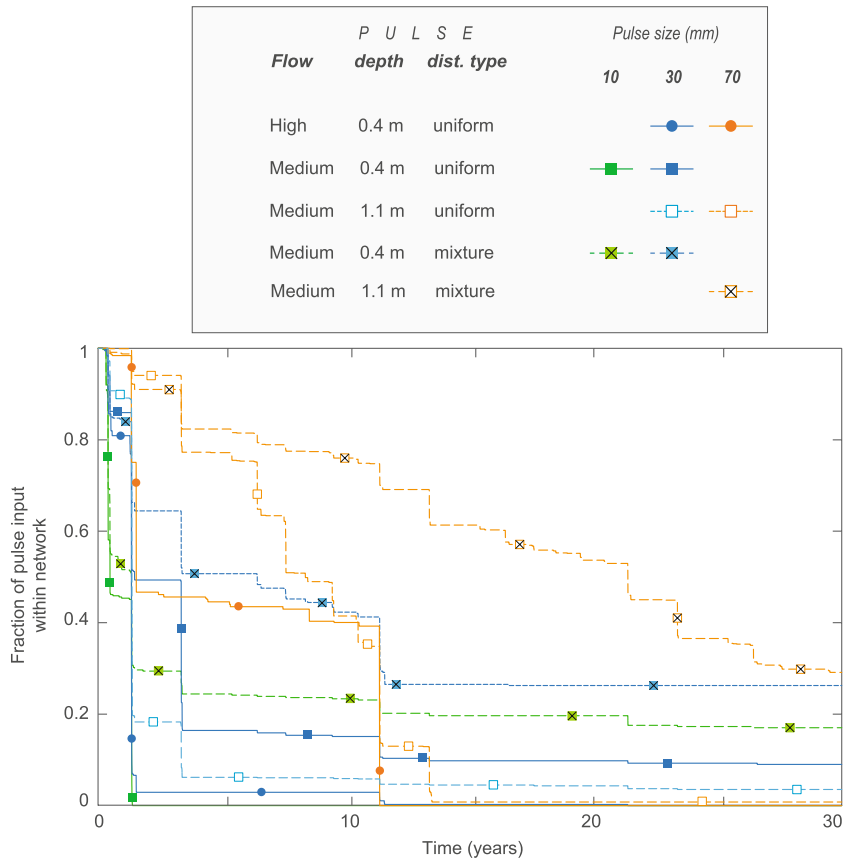

Figure 4. Movement of sediment pulses of different sizes (10, 30, and 70 mm), distribution type (uniform and mixed), and volume (0.4 and 1.1 m depth) through the mainstem Nisqually River under high and medium flow conditions.

4.2.1. Uniform and Mixed 10 mm Pulse

Changes in sediment depth from baseline (without pulse) are shown for uniform and mixed type pulses of 10 mm and 0.4 m depth under the medium flow condition (Figures 5a and 5b; and Figures 5e and 5f zoom in on Figures 5a and 5b, respectively). These model results show systemic initial incision (light brown colors generally before 1.2 year, Figures 5a and 5b), likely because the pulse is cutting off the background sediment supply that would have otherwise made it downstream. Then the pulse moves through the network, fairly coherently between 1.2 and 1.5 year (straight sloped dark blue lines in Figures 5e and 5f). This is the pulse itself causing aggradation and as a result of that pulse passing through (after 1.5 years), the bed sediment was mixed and mobilized in a way that results in longer term (but slight) incision (brown areas that dominate Figures 5a and 5b) compared to baseline. This prepulse incision and pulse aggradation were commonly observed in all of the following simulations as well. If we take horizontal slices through the zoomed space-time contours (e.g., dashed horizontal brown lines in Figures 5e and 5f at different times), we can see the location of the pulse along the model domain (Figures 5g and 5h).

To evaluate the dynamics more closely, we selected an example upstream reach (having approximately average width) at 7.6 km (brown dotted verticals in Figures 5a and 5b and plus sign in Figure 1). For both grain size distributions, the core of the pulse is marked in Figure 5d, before which (prepulse) the pulse reduces the baseline sediment supply. Maximum change from baseline is slightly higher for the uniform pulse (Figure 5d). The flow hydrograph is included as well to highlight that most fluctuations in bed sediment occur at high flow events. The timing of these impacts is, however, different, which is related to pulse arrival time. Pulse arrival time again depends on the dynamics of the flow and pulse size.

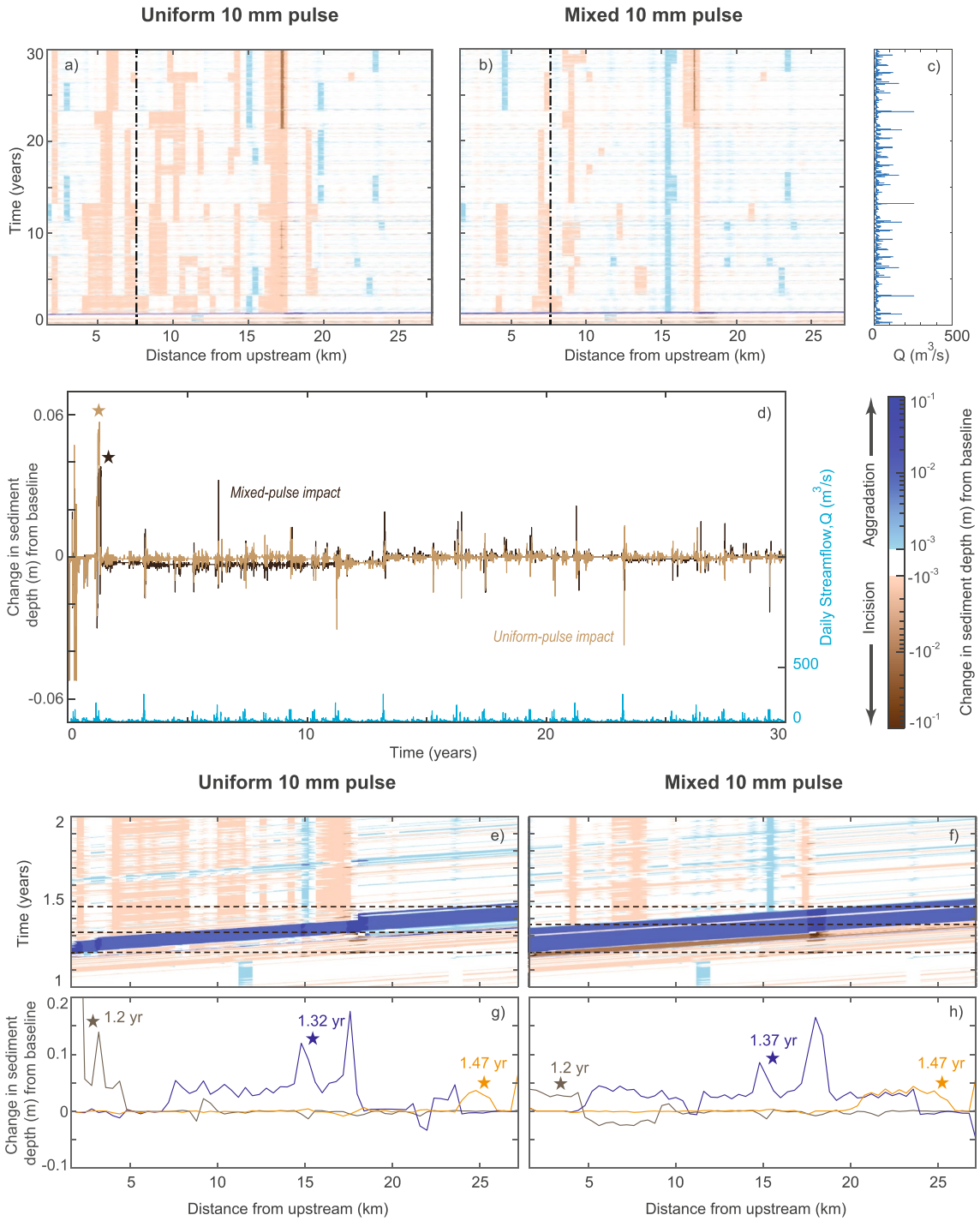

Figure 5. Comparison of the bed-elevation changes from uniform and mixed pulse of 10 mm median gravel size of 0.4 m depth for the medium flow condition. (a and b) Space-time contours of change in sediment depth from baseline due to uniform and mixed pulse. (c) Daily discharge at the upstream end of the model in medium flow condition. (d) Temporal changes in sediment depth from baseline at 7.6 km (location shown as dashed lines in (a and b)) due to uniform and mixed pulse. The star indicates the location of the pulse. (e and f) Space-time contours of change in sediment depth zoomed in on years 1–2 from (a and b), respectively. The narrow range in the *y*-axis helps to discern the movement of the pulse downstream. (g and h) Spatial changes in sediment depth from baseline at different times (horizontal dashed brown lines in [e and f]) also show the propagation of the pulse (indicated by star).

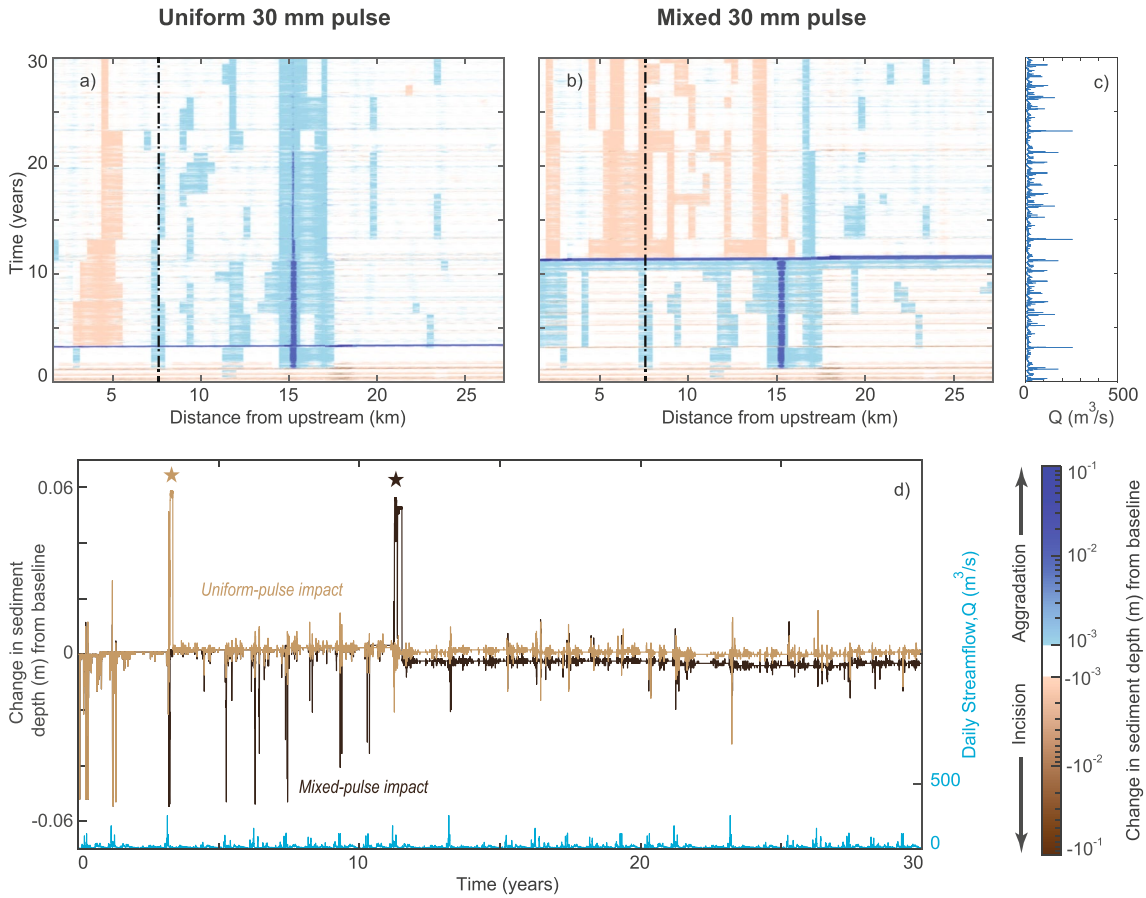

Figure 6. Comparison of the bed-elevation changes from uniform and mixed pulse of 30 mm median gravel size of 0.4 m depth for the medium flow condition. (a and b) Space-time contours of change in sediment depth from baseline due to uniform and mixed pulse. (c) Daily discharge at the upstream end of the model in medium flow condition. (d) Temporal changes in sediment depth from baseline at 7.6 km (location shown as dashed lines in [a and b]) due to uniform and mixed pulse, where the star indicates the location of the pulse.

Post-pulse change (after 1.5 years, Figures 5a and 5b) results in mostly incision (from baseline condition), which is greater for the uniform pulse, except for some aggradation in a low slope reach at 15.2 km. After passing through the narrow reaches (18 km), both pulses have little impact on the bed farther downstream. At location, 7.6 km after 1.5 years, the mixing and mobilizing of the bed sediment results in slight long-term incision, and this incision is marginally greater with the mixed pulse than the uniform pulse (Figure 5d). Model results showed that 70% of the pulse arrives at the outlet at around 1.5 years for both the uniform and mixed pulse (Figure 4). However, the total pulse volume arrives within 2 years for the uniform pulse, while only 83% of the mixed pulse leaves the system by the end of the 30-year simulation period.

4.2.2. Uniform and Mixed 30 mm Pulse

Changes in sediment depth from baseline are shown for uniform and mixed type pulses of 30 mm and 0.4 m depth under medium flow conditions (Figures 6a and 6b). Post-pulse change (after 3.5 years for the uniform pulse and at 11.5 years for the mixed pulse) results in mostly aggradation due to the uniform pulse (except in steep upstream reaches) and incision due to the mixed pulse (only up until 18.4 km; downstream of this narrow reach, there is aggradation in low sloped reaches). At location 7.6 km, there is post-pulse aggradation for the uniform pulse and incision for the mixed pulse (Figure 6d). Model results showed that 70% of the uniform pulse arrives at the outlet at 3.5 years and at 11.5 years for the mixed pulse (Figure 4). After the 30-year simulation, 75% of the mixed pulse and 90% of the uniform pulse was delivered to the outlet (Figure 4).

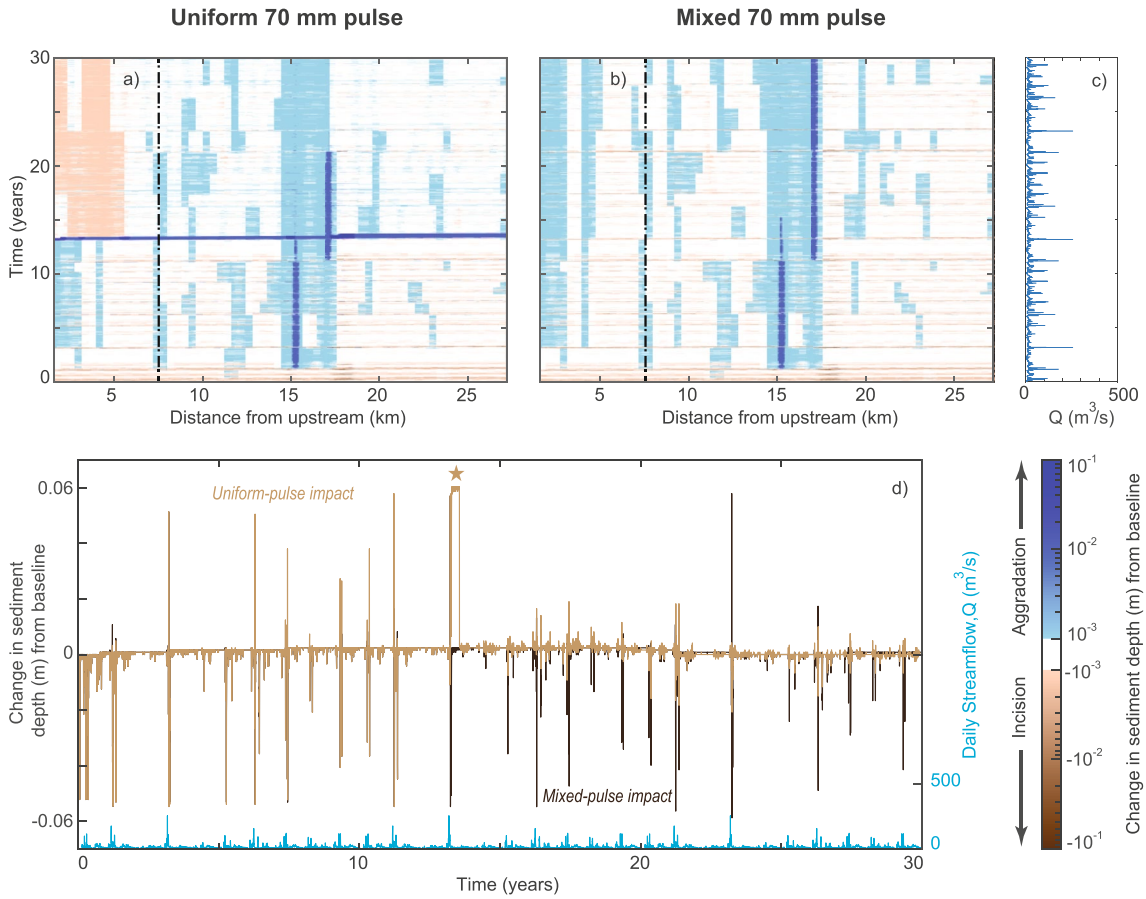

Figure 7. Comparison of the bed-elevation changes from uniform and mixed pulse with 70 mm median gravel size of 1.1 m depth for the medium flow condition. (a, b) Space-time contours of change in sediment depth from baseline due to uniform and mixed pulse. (c) Daily discharge at the upstream end of the model in medium flow condition. (d) Temporal changes in sediment depth from baseline at 7.6 km (location shown as dashed lines in [a and b]) due to uniform and mixed pulse, where the star indicates the location of the pulse.

4.2.3. Uniform and Mixed 70 mm Pulse

Changes in sediment depth from baseline were evaluated for uniform and mixed type pulses of 70 mm and 1.1 m depth under medium flow condition (Figure 7). Initial prepulse incision is dominant in both cases (bottom brown nearly straight lines, Figures 7a and 7b; negative fluctuations, Figure 7d). The incision continues for the uniform pulse (except in low slope reaches) until the pulse itself arrives downstream and aggrades the bed at around 13.5 years (Figure 7a). As it propagated downstream, the uniform pulse aggraded low slope reaches and incised steep upstream reaches (Figure 7a). In contrast, the 70 mm mixed pulse responded differently with no apparent peak in aggradation (Figures 7b and 7d). Recall, the 70 mm mixed pulse grain size distribution closely resembles the existing bed, so this pulse was expected to disperse slowly without a major mode of translation (Cui & Parker, 2005; Lisle et al., 1997, 2001; Sklar et al., 2009). What we observed was a more diffuse impact (Figure 7b), with some accumulation in lower-sloped reaches and bed-elevation fluctuations at flow peaks. Figure 4 shows that 70% of the uniform pulse arrived at the outlet at 11.5 years and at 28 years for the mixed pulse. These results do not show any marked pulse aggradation at 7.6 km due to the mixed pulse, but rather only show accumulation of the uniform pulse (at around 13.5 years, Figure 7d).

4.3. Summary of Pulse Impact

The results above (Sections 4.1–4.2, and in Supporting Information S1) showed the dynamic relation among pulse grain size, distribution type, and volume (depth), and streamflow hydrology. Here, we summarize the

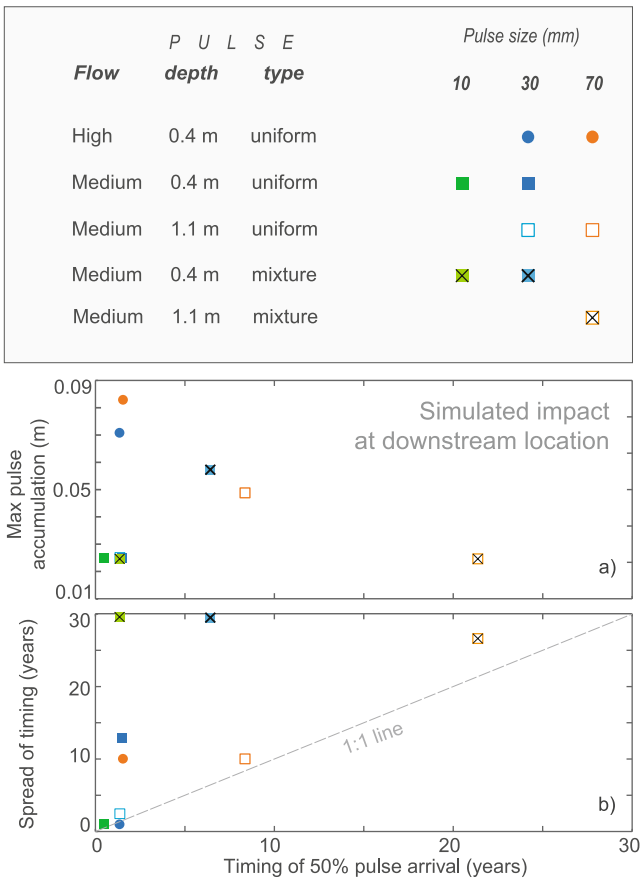

Figure 8. Simulated pulse impacts at downstream location (26.8 km; brown plus sign in Figure 1). (a) Maximum accumulation due to pulse and (b) spread of timing (difference in arrival time of 90% and 10% of the pulse) are plotted against the arrival time of 50% of the pulse.

maximum accumulation of the pulse, the spread of timing (difference between arrival time of 90% vs. 10% of the pulse), and arrival time of 50% of the pulse for all simulations at location 26.8 km (brown plus sign, Figure 1). We also present the average post-pulse impact (i.e., time-averaged change of sediment depth from baseline after pulse has passed a given location) for different sediment pulses along the river.

There are discernible patterns in the plot of 50% arrival time of the pulse vs. the magnitude of change in sediment depth (Figure 8a). The cluster of points around 2.5 cm pulse accumulation and low arrival timing might be limited by how the pulse spreads out over the reach geometry (Figure 8a). We see that the maximum pulse accumulations are greater for high flows (filled circles). For mixed pulses, we found that the finest gravel size (10 mm; roughly 0.15 of median bed gravel size) and coarsest gravel size (70 mm; roughly the same size as median bed gravel size) have the lowest pulse accumulations, even though the 10 mm pulse travels quickly and the 70 mm pulse disperses slowly. However, the mixed pulse with intermediate gravel size (30 mm; roughly 0.5 of the median bed gravel size) causes the greatest accumulation and has an intermediate arrival time compared to the other mixed pulses. This suggests that this intermediate size (roughly 0.5 of the median bed gravel size) is likely to have the largest downstream impact over the timescales studied here because finer sizes move through quickly and without significant alteration of the bed and coarser sizes disperse over timescales much longer than the 30-year simulations conducted here.

We find that, in general, arrival time increases with pulse grain size and mixed pulses spread out more in timing than uniform pulses (Figure 8b). For many of our simulated pulses with an appreciable spread in timing, we found that the arrival time distribution had a positive skewness (Figure 4), attributed to either the pulse mixing with the preexisting bed or a coarser tail that travels more slowly. For nearly every simulation (except the 30 mm pulse under high flow), the arrival time of the center of the pulse was of a shorter duration than that of the spread of timing (Figure 8b). For pulses with a long spread in timing, we found that timing of maximum change in bed elevation does not necessarily correspond to the timing of 50% pulse arrival (Figures 5d–7d). The contour plots of Figures 5–7 also showed that there was little difference in timing of the changes from upstream to downstream (because the brown and blue lines were nearly horizontal). This indicates that most of the pulses we have simulated were translation-dominated pulses for the mainstem of the Nisqually River (with the exception of the 70 mm mixed pulse, Figure 7). As our sediment pulses were mostly finer than the prepulse bed grain sizes, this translational behavior was expected (Sklar et al., 2009).

We present the time-averaged change in sediment depth from the baseline condition after the passage of the pulse through each location to summarize the complex post-pulse impact spatially (Figure 9). We also replot the river width and slope, and divide the network into distinct reaches to aid in interpretation. We qualitatively characterize five reaches: high slope-medium width, medium slope-high width, medium slope-low width, low slope-medium width, and low slope-high width (ordered from upstream to downstream). The flow change locations are at 14.4 and 23.6 km (light blue vertical dashed lines, Figure 9). The resulting average changes were greater for high flow compared to medium flow (solid dark blue and orange lines, Figure 9). The smallest pulse grain size (10 mm) caused average incision in high to medium slope and medium to low width reaches (centered at 5.2 and 17.6 km, respectively; solid and dashed green lines in Figure 9). Overall, post-pulse aggradation occurred where the channels widen (i.e., at transition locations at 8 and 23.6 km in Figure 9) due to a decrease in transport capacity (Czuba et al., 2017; Czuba, Magirl, et al., 2012; Gran & Czuba, 2017). This result highlights how the natural complexity of river structure (spatial distribution

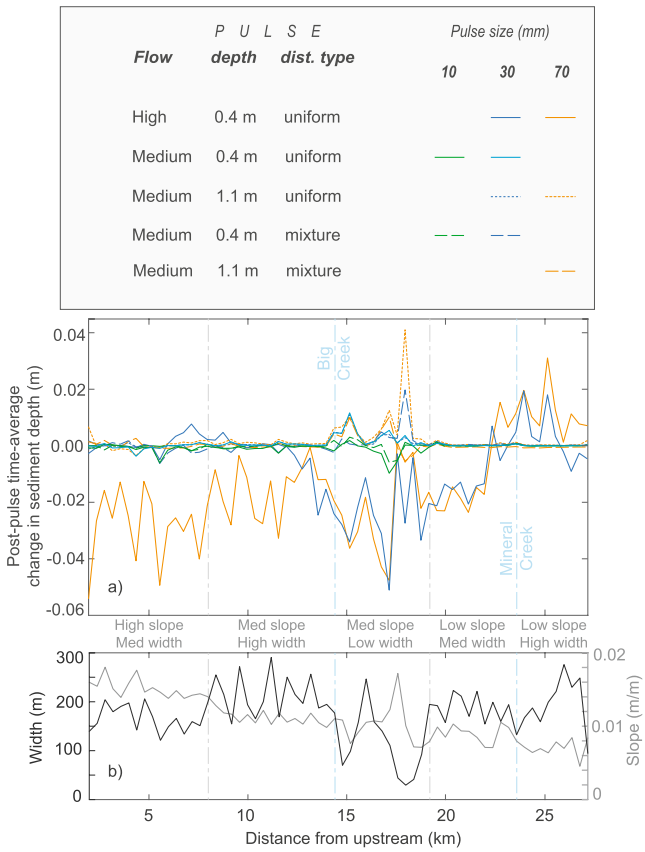

Figure 9. Simulated post-pulse time-averaged change in sediment depth (time-averaged change in sediment depth from the baseline condition after the pulse has passed each location) throughout the river network (a), along with variation in width and slope (b). The vertical dashed lines divide the network into five reaches; the light blue ones among them also indicate the locations of tributaries (Big Creek and Mineral Creek, in Figure 1).

of channel width and slope) plays an important role in any resulting aggradation or incision that occurs at any location due to propagation of a sediment pulse.

We compared simulated outlet volumes after the 30-year simulation period for all model runs (Figure 10b) to see how much bed sediment was mobilized and delivered to the outlet due to the pulse introduction. The change in outlet volume from the baseline condition (without pulse) was divided by the input pulse volume to normalize the results (Figure 10a). A normalized value greater than one indicates that an additional volume greater than the added pulse passed the outlet compared to the baseline simulation and highlights that the added pulse increased bed mobility. All pulses under the high flow condition and the 10 and 30 mm mixed pulses increased the mobility of the bed sediment (i.e., an amount of sediment greater than the sediment pulse addition was delivered to the outlet; Figures 10a and 10b). The large volume (1.1 m) uniform pulse runs delivered nearly the same amount of sediment that was added (Figures 10a and 10b). Simulations of the 10 and 30 mm pulses of small volume (0.4 m) with medium flow condition and the 70 mm mixed distribution pulse delivered less sediment to the outlet compared to baseline (Figures 10a and 10b). For these small volume uniform pulses, this was likely due to a reduced delivery of background sediment because of the presence of the pulse. For the 70 mm mixed distribution pulse, this was because most of that sediment did not arrive at the outlet in the 30-year simulation period. The uniform pulses alone do not appear to greatly mobilize bed sediment, because they cover the existing bed in a nearly uniform grain size that decreases mobility in the Wilcock and Crowe (2003) equations. Whereas the finer mixed pulses add a range of finer sizes to the bed grain size distribution and that together increases the mobility of the larger sizes without completely blanketing them in a uniform size range of finer sediment.

5. Discussion

5.1. Corroboration of Simulation Results With Previous Findings

Sediment pulses mix with bed sediment and affect bed-sediment composition and mobility in nonlinear ways (Humphries et al., 2012; Sklar et al., 2009; Venditti et al., 2010a, 2010b; Wooster et al., 2008). In general, our model results corroborated previous findings. Once emplaced, our model results showed that in all scenarios (Figures 5–7, Text S3 in Supporting Information S1) an initial prepulse incision occurs followed by sediment accumulation when the pulse arrives, consistent with Sklar et al. (2009). Post-pulse changes are more complex as they depend on nonlinear feedbacks among streamflow hydrology, channel structure, and mixing of pulse and bed sediment. We found that the maximum accumulation at any location occurred as a result of the pulse sediment, and after the passage of the pulse, the magnitude of changes in sediment depth was consistently small. General spatiotemporal patterns of long-term change in sediment depth suggest that sediment pulses tend to deposit in the wider and lower slope reaches (blue regions of the contour plots, Figures 5–7). Wider reaches, as well as reaches of transitional width (e.g., from a narrow to a wide channel), experience more average aggradation after the pulse has passed the reach compared to reaches with small to medium widths (Figure 9; Czuba, Magirl, et al., 2012). As the pulse grain sizes were (in most cases) smaller than the median bed grain size, a corresponding fining of the bed also occurred at these locations. Our simulations show that downstream changes in channel slope and width are strong controlling factors in pulse deposition, which is consistent with the findings of Major et al. (2012).

Sediment pulses finer than the median bed surface are transported faster and arrive downstream sooner than pulses that have a median grain size more similar to the bed surface (Figure 4; Cui & Parker, 2005;

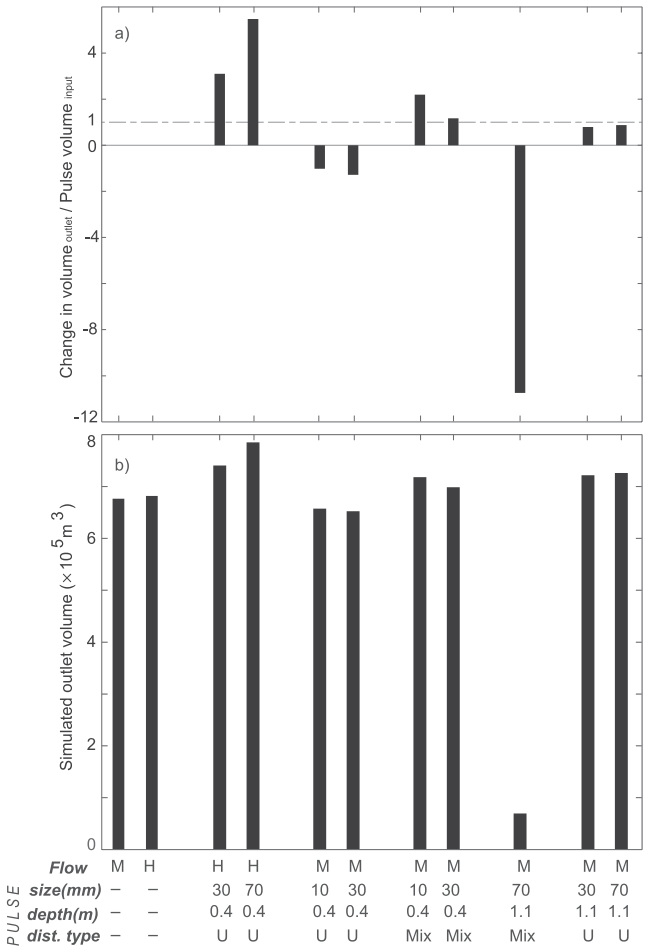

Figure 10. Simulated outlet volume for pulses of different size (10, 30, and 70 mm), depth (0.4 and 1.1 m), and distribution type (U and Mix, i.e., Uniform and Mixture) under medium and high flow (M and H) condition after the 30year simulation period. (a) The change in outlet volume from baseline normalized by the input pulse volume. That is, a value of one would indicate that an additional volume equivalent to the added pulse passed the outlet compared to the baseline simulation. (b) The total outlet volume, where the first two columns are baseline conditions for medium and high flow scenarios.

Cui, Parker, Lisle, et al., 2003; Cui, Parker, Pizzuto, et al., 2003; Sklar et al., 2009). An increase in the magnitude or frequency of sediment-transporting flows increases the sediment-transport capacity of rivers, resulting in sediment pulses that translate/disperse quicker (Cui & Parker, 2005) and arrive sooner (Figure 4). The 2-year recurrence interval flow, Q_2 (~105 m^3/s in the upstream end of modeled portion of the Nisqually), is often used as an approximation for the bankfull discharge (e.g., Snyder et al., 2013). The threshold for motion of D_{50} tends to occur at flows below the bankfull discharge (Parker, 1978). This is particularly true in high sediment supply channels such as the Nisqually (Pfeiffer & Finnegan, 2018; Pfeiffer et al., 2017). Thus, we expect Q_2 (and larger flows) should be sufficient to move a pulse grain size that is close to the median bed particle size (70 mm). In our models, we saw major changes occur when the flow was above Q_2 (Figures 4 and 7). For the 70 mm pulse, we saw that major changes occurred (at 1.2 and 3.2 years) when flow was significantly higher (~170 and ~250 m^3/s, respectively) than Q_2 (Figure 7). Gran and Czuba (2017) concluded that storage and dispersion become important when background sediment load is high. We saw gradual incision during the baseline simulation (Figure 3b), which reflects our relatively small background sediment supply. Additionally, because our pulse grain sizes were finer than the bed sediment (except the 70 mm pulses), we expected and observed translation of the sediment pulses (nearly horizontal lines in contour plots, Figures 5–7; Cui & Parker, 2005; Cui, Parker, Lisle, et al., 2003; Cui, Parker, Pizzuto, & Lisle, 2003; Lisle, 2008; Lisle et al., 1997, 2001; Sklar et al., 2009).

Our simulated model results showed that changes in sediment depth and bed grain size distributions were primarily influenced by sediment-pulse grain size and distribution type (Figures 5–7). The influence of streamflow hydrology was secondary and sediment-pulse volume (or depth) was tertiary, compared with the effects of pulse grain size (East et al., 2018; see Supporting Information S1). This finding is in contrast to modeling by Czuba, Magirl, et al. (2012), who increased pulse volume fivefold (compared to our lower threefold increase) and found the higher impact of pulse volume on the river bed compared to streamflow. The relative impact of flow and pulse volume, thus, will depend on the specifics of each. As expected, aggradation mostly occurred in reaches with low bedload transport capacity (e.g., Figure 9; Cui & Parker, 2005; Czuba, Magirl, et al., 2012). In general, our simulated pulses caused slight long-term aggradation from baseline, but when the median pulse grain size was small compared to the bed sediment (10 mm pulse, roughly 0.15 of the median bed gravel size; Figure 5 and Text S3 in Supporting Information S1), incision dominated. One possible reason is that the mixing of the finer pulse with the pre-existing bed sediment modifies the bed sediment size distribution in a way that leads to overall increased sediment transport (Venditti et al., 2010b; Wilcock & Crowe, 2003). Our larger volume pulses traveled faster through the system than our smaller volume pulses. This occurred because the smaller volume pulse more fully mixed with the bed material compared to the larger volume pulse and the larger volume pulse also further increased the local channel slope to increase the transport rate.

5.2. Differences Between Uniform and Mixed Grain Size Pulse Behavior

Our model simulations demonstrated how mixed-size sediment pulses, which are common in natural and human-influenced riverscapes, may affect downstream bed elevations, grain size, and sediment transport differently than uniform-sized sediment pulses, which have been more commonly studied. The arrival time

of 50% of the pulse was nearly the same for the uniform and mixed pulses (finer than the bed), but the coarse tail of the mixed pulse traveled slower (Figure 4). We also found that incision due to a finer pulse was more prevalent for a uniform pulse compared to a mixed pulse (Figure 5). This is likely because the mixed pulse dispersed slowly compared to the uniform pulse that translated with less spread, which led to greater magnitude change. When the median grain size was close to that of the bed, the mixed pulse traveled very slowly in the system and resulted in a more diffuse impact compared to the uniform pulse (Figure 7). In general, the finer fraction of the mixed pulse traveled quickly and interacted with the bed in downstream locations first, while the coarser fraction traveled very slowly; thus, the pattern of bed-elevation change was more variable with a mixed pulse than a uniform pulse.

Model simulations included three different sized mixed pulses, where the mixed pulse with an intermediate gravel size (roughly 0.5 of the median bed gravel size) caused the largest downstream aggradation. As expected, the finer mixed pulse caused less aggradation, but when the median gravel size of the mixed pulse was roughly the same size as that of bed (70 mm), we found similarly low aggradation (Figure 8a; Czuba, Magirl, et al., 2012; Sklar et al., 2009). The mixed pulse with 70 mm median grain size dispersed slowly (Figure 4), which allowed small and finer portions of the pulse to move through the system without much deposition. This novel finding suggests that there is an intermediate median grain size for mixed-size sediment pulses (here, roughly 0.5 of the median bed size) that may result in the largest downstream bed impacts, because finer sizes are transported through too quickly and coarser sizes disperse too slowly to exert influence over year to decadal timescales.

Another noteworthy result from the simulations is that mixed-size pulses with median grain size smaller than the bed increased bed mobility more than pulses of uniform-size distributions (Figure 10a). This is because finer mixed pulses incorporate a range of fine grain sizes into the bed and increase the mobility of larger grains without completely blanketing them in a uniformly fine layer of sediment. Whereas, mixed-size pulses with size and distribution equivalent to the preexisting bed, disperse very slowly, reduce background sediment supply, and limit sediment export (70 mm mixed pulse, Figures 10a and 10b). Thus, to increase bed mobility downstream, rather than adding a relatively fine and uniformly distributed pulse (Arnaud et al., 2017; Gaeuman et al., 2017; Venditti et al., 2010b), our model results suggest that bed mobility would be enhanced if the pulse has a wide grain size distribution.

5.3. Limitations and Future Improvements

While this study only focused on the one-dimensional aspects of sediment-pulse evolution, the spatial complexity of rivers can influence patterns of sediment-pulse evolution (Kasprak et al., 2015; Nelson & Dubé, 2016; Recking et al., 2016). Our simulated sediment depths are of a sediment volume deposited uniformly over the entire width of 400 m sections of river, so in reality, we would expect locally greater accumulations to occur. Local or reach-scale topography can affect how sediment pulses are transported through a reach and affect how well bedload equations developed from flume studies translate to field scale (Recking et al., 2016). Sediment pulses tend to accumulate on point bars and their growth can modify flow patterns and lead to more active channel migration (Humphries et al., 2012; Parker et al., 2011). Additionally, sediment can fill pools or locally deposit behind large woody debris, further complicating sediment-pulse evolution (Harrison et al., 2018; Major et al., 2012; Ryan et al., 2014; Wohl & Scott, 2017). The model used in this study does not currently consider time-varying channel width, and the interactions among bank supply, bed structure, and lateral sediment exchange, as does the MAST-1D model.

Another major limitation of the current work was that the model was not able to maintain a bed material with enough sand to match the measured grain size distributions from gravel bars. This means that in reality, for the Nisqually River, bed sediment is probably more mobile and would transport downstream faster than we have predicted. When sand content was high (above 5%), the model flushed out most of the sand from the network. As a result, we noticed bed incision and corresponding bed coarsening at flow peaks (Figure 3). Without a separate transport equation for sand, as is done in the TUGS model, our present model was unable to effectively characterize sand transport. While our model was able to route a gravel mixture, the inclusion of a sand transport equation would make it more robust in simulating the transport of combined gravel and sand mixtures, particularly in the challenging case of the Nisqually River.

Our model results are applicable to sediment pulses on the order of 10,000 m^3, such as from small dam removals (<10 m high, delivering less than 10,000 m^3; Bellmore et al., 2017; Foley et al., 2017; Major et al., 2017) and gravel augmentation (23,000 m^3; Arnaud et al., 2017). These are the sediment-pulse volumes typically encountered by river managers. In the past few years, more data sets of larger sediment inputs, primarily from larger dam removals (Cashman et al., 2021; East et al., 2015, 2018; Harrison et al., 2018; Major et al., 2012; Pace et al., 2017; Ritchie et al., 2018; Warrick et al., 2015) and modeling studies using these data sets (Cui et al., 2014, 2019; De Rego et al., 2020) have appeared in the literature. In the future, more directly testing an updated model against these data sets would provide a robust validation of large sediment-pulse movement in rivers.

6. Summary

This study utilized existing physical measurements of the Nisqually River for applying a previous Lagrangian, bed-material sediment transport model. We sought to investigate how perturbations in sediment supply, modeled as sediment pulses in this river system, dictate the bed response. Specifically, we were interested in showing how mixed-size sediment pulses, which are common in natural and human-influenced river systems, affect downstream bed elevations, grain size, and sediment transport differently than uniform-sized sediment pulses, which have been commonly studied. Our model results are applicable to sediment inputs on the order of 10,000 m^3. Simulation results pointed to an initial prepulse incision followed by sediment accumulation at the time of pulse arrival, and then, complex post-pulse changes. Sediment pulses were strongly translational when pulses were finer than the existing bed material. Introduced pulses caused slight long-term accumulation (especially at downstream reaches with low transport capacity) in general, but if the pulse grain size was much finer than the bed sediment (roughly 0.15 of the median bed gravel size), incision may occur due to increased bed-sediment mobility. We saw that the flow hydrograph had a strong control over the timing of these sedimentologic changes.

We found that pulse distribution type (uniform or mixture) was an important influence on the channel bed. Results of model simulations indicated that a mixed pulse with an intermediate gravel size (roughly 0.5 of the median bed gravel size) may cause higher downstream accumulations compared to a mixed pulse with a median gravel size much finer than or equivalent to that of the bed because either finer sizes move through quickly or coarser sizes disperse slowly. Furthermore, mixed-distribution pulses with smaller median grain sizes than the bed increase bed mobility more than uniform-distribution pulses. This is because finer mixed pulses add a range of fine grain sizes to the bed, thereby increasing the mobility of the larger sizes without covering them in a uniformly fine layer of sediment.

This research furthers our understanding of the space-time evolution and downstream effects of sediment pulses in gravel-bedded rivers, and contributes to river management by assessing potential fluvial geomorphic response due to discrete inputs of sediment that could be from natural or anthropogenic sources. Finally, this work revealed that incorporating a sand transport equation into our model in the future will be necessary in order to make it more robust for simulating the transport of combined gravel and sand mixtures. Future model improvements could also include channel-floodplain exchange of water and sediment and future validation should take advantage of recent data sets describing river response to dam removal.

Data Availability Statement

Data sets for this research are available at: https://doi.org/10.4211/hs.1a6f403d90a542f6b0770d19ee5e8341. Additional versions of the model are freely available in Matlab from Czuba (2018) via the Community Surface Dynamics Modeling System (https://csdms.colorado.edu/wiki/Model:River_Network_Bed-Material_Sediment) or in Python from Pfeiffer et al. (2020) via Landlab.

Acknowledgments
This work was partially supported by the National Science Foundation (NSF-EAR 1848672 to J. A. Czuba and NSF-EAR 1848667 to B. P. Murphy and P. Belmont), the Virginia (J. A. Czuba) and Utah (P. Belmont) Agricultural Experiment Stations, and the USDA Hatch program (1017457 to J. A. Czuba). The authors thank three anonymous reviewers, Associate Editor (Luca Solari), and Editor (Amy East) for providing thoughtful and insightful comments that helped improve the presentation and sharpen the focus of our work.

References

An, C., Cui, Y., Fu, X., & Parker, G. (2017). Gravel-bed river evolution in earthquake-prone regions subject to cycled hydrographs and repeated sediment pulses. *Earth Surface Processes and Landforms*, *42*(14), 2426–2438. https://doi.org/10.1002/esp.4195

Anderson, S., & Pitlick, J. (2014). Using repeat lidar to estimate sediment transport in a steep stream. *Journal of Geophysical Research: Earth Surface*, *119*(3), 621–643. https://doi.org/10.1002/2013JF002933

Arnaud, F., Piégay, H., Béal, D., Collery, P., Vaudor, L., & Rollet, A. J. (2017). Monitoring gravel augmentation in a large regulated river and implications for process-based restoration. *Earth Surface Processes and Landforms*, *42*(13), 2147–2166. https://doi.org/10.1002/esp.4161

Ashworth, P. J., & Ferguson, R. I. (1989). Size-selective entrainment of bed load in gravel bed streams. *Water Resources Research*, *25*(4), 627–634. https://doi.org/10.1029/WR025i004p00627

Bellmore, J. R., Duda, J. J., Craig, L. S., Greene, S. L., Torgersen, C. E., Collins, M. J., & Vittum, K. (2017). Status and trends of dam removal research in the United States. *Wiley Interdisciplinary Reviews: Water*, *4*(2), e1164. https://doi.org/10.1002/wat2.1164

Benda, L., Andras, K., Miller, D., & Bigelow, P. (2004). Confluence effects in rivers: Interactions of basin scale, network geometry, and disturbance regimes. *Water Resources Research*, *40*(5). https://doi.org/10.1029/2003WR002583

Benda, L., & Dunne, T. (1997a). Stochastic forcing of sediment routing and storage in channel networks. *Water Resources Research*, *33*(12), 2865–2880. https://doi.org/10.1029/97WR02387

Benda, L., & Dunne, T. (1997b). Stochastic forcing of sediment supply to channel networks from landsliding and debris flow. *Water Resources Research*, *33*(12), 2849–2863. https://doi.org/10.1029/97WR02388

Cashman, M. J., Gellis, A. C., Boyd, E., Collins, M. J., Anderson, S. W., McFarland, B. D., & Ryan, A. M. (2021). Channel response to a dam-removal sediment pulse captured at high-temporal resolution using routine gage data. *Earth Surface Processes and Landforms*, *46*(6), 1145–1159. https://doi.org/10.1002/esp.5083

Castro-Bolinaga, C. F., Diplas, P., & Bodnar, R. J. (2020). Modeling hydro-morphodynamic processes during the propagation of fluvial sediment pulses: A physics-based framework. *Journal of Geophysical Research: Earth Surface*, *125*(12), e2020JF005722. https://doi.org/10.1029/2020JF005722

Copeland, E. A. (2009). *Recent periglacial debris flows from Mount Rainier* (M.S. thesis). Oregon State University.

Crandell, D. R. (1971). *Postglacial lahars from Mount Rainier Volcano, Washington* (Vol. 677, p. 75). US Geological Survey Professional Paper.

Cui, Y. (2007). The unified gravel-sand (TUGS) model: Simulating sediment transport and gravel/sand grain size distributions in gravel-bedded rivers. *Water Resources Research*, *43*, W10436. https://doi.org/10.1029/2006WR005330

Cui, Y., Collins, M. J., Andrews, M., Boardman, G. C., Wooster, J. K., Melchior, M., & McClain, S. (2019). Comparing 1D sediment transport modeling with field observations: Simkins Dam removal case study. *International Journal of River Basin Management*, *17*(2), 185–197. https://doi.org/10.1080/15715124.2018.1508024

Cui, Y., & Parker, G. (2005). Numerical model of sediment pulses and sediment-supply disturbances in mountain rivers. *Journal of Hydraulic Engineering*, *131*(8), 646–656. https://doi.org/10.1061/(ASCE)0733-9429(2005)131:8(646)

Cui, Y., Parker, G., Braudrick, C., Dietrich, W. E., & Cluer, B. (2006a). Dam removal express assessment models (DREAM). Part 1: Model development and validation. *Journal of Hydraulic Research*, *44*(3). https://doi.org/10.1080/00221686.2006.9521683

Cui, Y., Parker, G., Braudrick, C., Dietrich, W. E., & Cluer, B. (2006b). Dam removal express assessment models (DREAM). Part 2: Sample runs/sensitivity tests. *Journal of Hydraulic Research*, *44*(3). https://doi.org/10.1080/00221686.2006.9521684

Cui, Y., Parker, G., Lisle, T. E., Gott, J., Hansler-Ball, M. E., Pizzuto, J. E., et al. (2003). Sediment pulses in mountain rivers: 1. Experiments. *Water Resources Research*, *39*(9), 1239. https://doi.org/10.1029/2002WR001803

Cui, Y., Parker, G., Pizzuto, J., & Lisle, T. E. (2003). Sediment pulses in mountain rivers: 2. Comparison between experiments and numerical predictions. *Water Resources Research*, *39*(9), 1240. https://doi.org/10.1029/2002WR001805

Cui, Y., & Wilcox, A. (2008). Development and application of numerical models of sediment transport associated with dam removal. In M. H. Garcia (Ed.), *Sedimentation engineering: Processes, measurements, modeling, and practice, American Society of Civil Engineers manuals and reports on engineering practice* (Vol. 110, pp. 995–1020). ASCE. https://doi.org/10.1061/9780784408148.ch23

Cui, Y., Wooster, J. K., Braudrick, C. A., & Orr, B. K. (2014). Lessons learned from sediment transport model predictions and long-term post-removal monitoring: Marmot Dam removal project on the Sandy River in Oregon. *Journal of Hydraulic Engineering*, *140*(9), 04014044. https://doi.org/10.1061/(ASCE)HY.1943-7900.0000894

Czuba, C. R., Randle, T. J., Bountry, J. A., Magirl, C. S., Czuba, J. A., Curran, C. A., & Konrad, C. P. (2011). *Anticipated sediment delivery to the lower Elwha River during and following dam removal*. US Department of the Interior, US Geological Survey.

Czuba, J. A. (2018). A Lagrangian framework for exploring complexities of mixed-size sediment transport in gravel-bedded river networks. *Geomorphology*, *321*, 146–152. https://doi.org/10.1016/j.geomorph.2018.08.031

Czuba, J. A., Czuba, C. R., Magirl, C. S., & Voss, F. D. (2010). Channel-conveyance capacity, channel change, and sediment transport in the lower Puyallup, White, and Carbon Rivers, western Washington. *U.S. Geological Survey Scientific Investigations Report 2010–5240*, (p. 104).

Czuba, J. A., & Foufoula-Georgiou, E. (2014). A network-based framework for identifying potential synchronizations and amplifications of sediment delivery in river basins. *Water Resources Research*, *50*(5), 3826–3851. https://doi.org/10.1002/2013WR014227

Czuba, J. A., Foufoula-Georgiou, E., Gran, K. B., Belmont, P., & Wilcock, P. R. (2017). Interplay between spatially-explicit sediment sourcing, hierarchical river-network structure, and in-channel bed-material sediment transport and storage dynamics. *Journal of Geophysical Research: Earth Surface*, *122*(5), 1090–1120. https://doi.org/10.1002/2016JF003965

Czuba, J. A., Magirl, C. S., Czuba, C. R., Curran, C. A., Johnson, K. H., Olsen, T. D., et al. (2012). Geomorphic analysis of the river response to sedimentation downstream of Mount Rainier, Washington. *U.S. Geological Survey Open-File Report 2012–1242*, (p. 134).

Czuba, J. A., Olsen, T. D., Czuba, C. R., Magirl, C. S., & Gish, C. C. (2012). Changes in sediment volume in Alder Lake, Nisqually River basin, Washington, 1945–2011. *U.S. Geological Survey Open-File Report 2012–1068*, (p. 30).

De Rego, K., Lauer, J. W., Eaton, B., & Hassan, M. (2020). A decadal-scale numerical model for wandering, cobble-bedded rivers subject to disturbance. *Earth Surface Processes and Landforms*, *45*(4), 912–927. https://doi.org/10.1002/esp.4784

Dingle, E. H., Attal, M., & Sinclair, H. D. (2017). Abrasion-set limits on Himalayan gravel flux. *Nature*, *544*(7651), 471–474. https://doi.org/10.1038/nature22039

Dow, S., Snyder, N. P., Ouime, W. B., Martini, A. M., Yellen, B., Woodruff, J. D., et al. (2020). Estimating the timescale of fluvial response to anthropogenic disturbance using two generations of dams on the South River, Massachusetts, USA. *Earth Surface Processes and Landforms*, *45*(10), 2380–2393. https://doi.org/10.1002/esp.4886

East, A. E., Logan, J. B., Mastin, M. C., Ritchie, A. C., Bountry, J. A., Magirl, C. S., & Sankey, J. B. (2018). Geomorphic evolution of a gravel-bed river under sediment-starved vs. sediment-rich conditions: River response to the world's largest dam removal. *Journal of Geophysical Research: Earth Surface*, *123*(12), 3338–3369. https://doi.org/10.1029/2018JF004703

East, A. E., Pess, G. R., Bountry, J. A., Magirl, C. S., Ritchie, A. C., Logan, J. B., et al. (2015). Large-scale dam removal on the Elwha River, Washington, USA: River channel and floodplain geomorphic change. *Geomorphology*, *246*, 687–786. https://doi.org/10.1016/j.geomorph.2014.08.028

Foley, M. M., Bellmore, J. R., O'Connor, J. E., Duda, J. J., East, A. E., Grant, G. E., et al. (2017). Dam removal: Listening in. *Water Resources Research*, *53*(7), 5229–5246. https://doi.org/10.1002/2017WR020457

Gaeuman, D., Stewart, R., Schmandt, B., & Pryor, C. (2017). Geomorphic response to gravel augmentation and high-flow dam release in the Trinity River, California. *Earth Surface Processes and Landforms*, *42*(15), 2523–2540. https://doi.org/10.1002/esp.4191

Garcia, M. H. (2008). Sediment transport and morphodynamics. In *Sedimentation engineering: Processes, measurements, modeling, and practice* (pp. 21–163). https://doi.org/10.1061/9780784408148.ch02

Gran, K. B., & Czuba, J. A. (2017). Sediment pulse evolution and the role of network structure. *Geomorphology*, *277*, 17–30. https://doi.org/10.1016/j.geomorph.2015.12.015

Harrison, L. R., East, A. E., Smith, D. P., Logan, J. B., Bond, R. M., Nicol, C. L., et al. (2018). River response to large-dam removal in a Mediterranean hydroclimatic setting: Carmel River, California, USA. *Earth Surface Processes and Landforms*, *43*(15), 3009–3021. https://doi.org/10.1002/esp.4464

Humphries, R., Venditti, J. G., Sklar, L. S., & Wooster, J. K. (2012). Experimental evidence for the effect of hydrographs on sediment pulse dynamics in gravel-bedded rivers. *Water Resources Research*, *48*, W01533. https://doi.org/10.1029/2011WR010419

James, L. A. (2010). Secular sediment waves, channel bed waves, and legacy sediment. *Geography Compass*, *4*(6), 576–598. https://doi.org/10.1111/j.1749-8198.2010.00324.x

Kasprak, A., Wheaton, J. M., Ashmore, P. E., Hensleigh, J. W., & Peirce, S. (2015). The relationship between particle travel distance and channel morphology: Results from physical models of braided rivers. *Journal of Geophysical Research: Earth Surface*, *120*(1), 55–74. https://doi.org/10.1002/2014JF003310

Keulegan, G. H. (1938). *Laws of turbulent flow in open channels* (Vol. 21, pp. 707–741). National Bureau of Standards. https://doi.org/10.6028/jres.021.039

Lauer, J. W., & Parker, G. (2008). Modeling framework for sediment deposition, storage, and evacuation in the floodplain of a meandering river: Theory. *Water Resources Research*, *44*, W04425. https://doi.org/10.1029/2006WR005528

Lauer, J. W., Viparelli, E., & Piégay, H. (2016). Morphodynamics and sediment tracers in 1D (MAST-1D): 1D sediment transport that includes exchange with an off-channel sediment reservoir. *Advances in Water Resources*, *93*, 135–149. https://doi.org/10.1016/j.advwatres.2016.01.012

Legg, N. T., Meigs, A. J., Grant, G. E., & Kennard, P. (2014). Debris flow initiation in proglacial gullies on Mount Rainier, Washington. *Geomorphology*, *226*, 249–260. https://doi.org/10.1016/j.geomorph.2014.08.003

Lisle, T. E. (2008). The evolution of sediment waves influenced by varying transport capacity in heterogeneous rivers. In H. Habersack, H. Piegay, & M. Rinaldi (Eds.), *Gravel bed rivers VI: From process understanding to river restoration* (p. 443–472). Elsevier. https://doi.org/10.1016/S0928-2025(07)11136-6

Lisle, T. E., Cui, Y., Parker, G., Pizzuto, J. E., & Dodd, A. M. (2001). The dominance of dispersion in the evolution of bed material waves in gravel-bed rivers. *Earth Surface Processes and Landforms*, *26*, 1409–1420. https://doi.org/10.1002/esp.300

Lisle, T. E., Pizzuto, J. E., Ikeda, H., Iseya, F., & Kodama, Y. (1997). Evolution of a sediment wave in an experimental channel. *Water Resources Research*, *33*(8), 1971–1981. https://doi.org/10.1029/97WR01180

Major, J. J., East, A. E., O'Connor, J. E., Grant, G. E., Wilcox, A. C., Magirl, C. S., et al. (2017). Geomorphic responses to dam removal in the United States—A two-decade perspective. *Gravel-Bed Rivers*, *10*(9781118971437), 355–383. https://doi.org/10.1002/9781118971437.ch13

Major, J. J., O'Connor, J. E., Podolak, C. J., Keith, M. K., Grant, G. E., Spicer, K. R., et al. (2012). *Geomorphic response of the Sandy River, Oregon, to removal of Marmot Dam* (p. 64). USGS Professional Paper 1792.

Moody, J. A., & Martin, D. A. (2004). Wildfire impacts on reservoir sedimentation in the western United States. *Proceedings of the Ninth International Symposium on River Sedimentation* (pp. 1095–1102). Tsinghua University Press China.

Murphy, B. P., Czuba, J. A., & Belmont, P. (2019). Post-wildfire sediment cascades: A modeling framework linking debris flow generation and network-scale sediment routing. *Earth Surface Processes and Landforms*, *44*(11), 2126–2140. https://doi.org/10.1002/esp.4635

Murphy, B. P., Yocom, L. L., & Belmont, P. (2018). Beyond the 1984 perspective: Narrow focus on modern wildfire trends underestimates future risks to water security. *Earth's Future*, *6*(11), 1492–1497. https://doi.org/10.1029/2018EF001006

Nelson, A., & Dubé, K. (2016). Channel response to an extreme flood and sediment pulse in a mixed bedrock and gravel-bed river. *Earth Surface Processes and Landforms*, *41*(2), 178–195. https://doi.org/10.1002/esp.3843

O'Connor, J. E., Mangano, J. F., Anderson, S. W., Wallick, J. R., Jones, K. L., & Keith, M. K. (2014). Geologic and physiographic controls on bed-material yield, transport, and channel morphology for alluvial and bedrock rivers, western Oregon. *Geological Society of America Bulletin*, *126*(3–4), 377–397. https://doi.org/10.1130/b30831.1

Pace, K. M., Tullos, D., Walter, C., Lancaster, S., & Segura, C. (2017). Sediment pulse behaviour following dam removal in gravel-bed rivers. *River Research and Applications*, *33*(1), 102–112. https://doi.org/10.1002/rra.3064

Paola, C., Parker, G., Seal, R., Sinha, S. K., Southard, J. B., & Wilcock, P. R. (1992). Downstream fining by selective deposition in a laboratory flume. *Science*, *258*(5089), 1757–1760. https://doi.org/10.1126/science.258.5089.1757

Parker, G. (1978). Self-formed straight rivers with equilibrium banks and mobile bed. Part 2. The gravel river. *Journal of Fluid Mechanics*, *89*(1), 127–146. https://doi.org/10.1017/S0022112078002505

Parker, G. (1991). Selective sorting and abrasion of river gravel. I: Theory. *Journal of Hydraulic Engineering*, *117*(2), 131–147. https://doi.org/10.1061/(ASCE)0733-9429(1991)117:2(131)

Parker, G., Shimizu, Y., Wilkerson, G. V., Eke, E. C., Abad, J. D., Lauer, J. W., et al. (2011). A new framework for modeling the migration of meandering rivers. *Earth Surface Processes and Landforms*, *36*(1), 70–86. https://doi.org/10.1002/esp.2113

Pfeiffer, A. M., Barnhart, K. R., Czuba, J. A., & Hutton, E. (2020). NetworkSedimentTransporter: A Landlab component for bed material transport through river networks. *Journal of Open Source Software*, *5*(53), 2341. https://doi.org/10.21105/joss.02341

Pfeiffer, A. M., Collins, B. D., Anderson, S. W., Montgomery, D. R., & Istanbulluoglu, E. (2019). River bed elevation variability reflects sediment supply, rather than peak flows, in the uplands of Washington State. *Water Resources Research*, *55*(8), 6795–6810. https://doi.org/10.1029/2019WR025394

Pfeiffer, A. M., & Finnegan, N. J. (2018). Regional variation in gravel riverbed mobility, controlled by hydrologic regime and sediment supply. *Geophysical Research Letters*, *45*(7), 3097–3106. https://doi.org/10.1002/2017GL076747

Pfeiffer, A. M., Finnegan, N. J., & Willenbring, J. K. (2017). Sediment supply controls equilibrium channel geometry in gravel rivers. *Proceedings of the National Academy of Sciences*, *114*(13), 3346–3351. https://doi.org/10.1073/pnas.1612907114

PSLC, Puget Sound LiDAR Consortium. (2012). *2008–2009 Lewis County LiDAR Project*. Retrieved from http://pugetsoundlidar.ess.washington.edu/

Recking, A., Piton, G., Vazquez-Tarrio, D., & Parker, G. (2016). Quantifying the morphological print of bedload transport. *Earth Surface Processes and Landforms*, *41*(6), 809–822. https://doi.org/10.1002/esp.3869

Ritchie, A. C., Warrick, J. A., East, A. E., Magirl, C. S., Stevens, A. W., Bountry, J. A., et al. (2018). Morphodynamic evolution following sediment release from the world's largest dam removal. *Scientific Reports*, *8*(1), 1–13. https://doi.org/10.1038/s41598-018-30817-8

Ryan, S. E., Bishop, E. L., & Daniels, J. M. (2014). Influence of large wood on channel morphology and sediment storage in headwater mountain streams, Fraser Experimental Forest, Colorado. *Geomorphology*, *217*, 73–88. https://doi.org/10.1016/j.geomorph.2014.03.046

Sankey, J. B., Kreitler, J., Hawbaker, T. J., McVay, J. L., Miller, M. E., Mueller, E. R., et al. (2017). Climate, wildfire, and erosion ensemble foretells more sediment in western USA watersheds. *Geophysical Research Letters*, *44*, 8884–8892. https://doi.org/10.1002/2017GL073979

Schmitt, R. J., Bizzi, S., Castelletti, A. F., & Kondolf, G. M. (2018). Stochastic modeling of sediment connectivity for reconstructing sand fluxes and origins in the unmonitored Se Kong, Se San, and Sre Pok tributaries of the Mekong River. *Journal of Geophysical Research: Earth Surface*, *123*(1), 2–25. https://doi.org/10.1002/2016JF004105

Sklar, L. S., Fadde, J., Venditti, J. G., Nelson, P., Wydzga, M. A., Cui, Y., & Dietrich, W. E. (2009). Translation and dispersion of sediment pulses in flume experiments simulating gravel augmentation below dams. *Water Resources Research*, *45*, W08439. https://doi.org/10.1029/2008WR007346

Snyder, N. P., Nesheim, A. O., Wilkins, B. C., & Edmonds, D. A. (2013). Predicting grain size in gravel-bedded rivers using digital elevation models: Application to three Maine watersheds. *Geological Society of America Bulletin*, *125*(1–2), 148–163. https://doi.org/10.1130/B30694.1

Sutherland, D. G., Hansler-Ball, M., Hilton, S. J., & Lisle, T. E. (2002). Evolution of a landslide induced sediment wave in the Navarro River, California. *Geological Society of America Bulletin*, *114*(8), 1036–1048. https://doi.org/10.1130/0016-7606(2002)114<1036:EOALIS>2.0.CO;2

U.S. Department of Agriculture. (2011). *National Agricultural Imagery Program*. U.S. Department of Agriculture. Retrieved from http://www.fsa.usda.gov/FSA/apfoapp?area=home&subject=prog&topic=nai

USGS, U. S. Geological Survey. (2021). *USGS 12082500, Nisqually River near National, WA*. Retrieved from https://waterdata.usgs.gov/nwis/inventory/?site_no=12082500&agency_cd=USGS

Venditti, J. G., Dietrich, W. E., Nelson, P. A., Wydzga, M. A., Fadde, J., & Sklar, L. (2010a). Effect of sediment pulse grain size on sediment transport rates and bed mobility in gravel bed rivers. *Journal of Geophysical Research*, *115*, F03039. https://doi.org/10.1029/2009JF001418

Venditti, J. G., Dietrich, W. E., Nelson, P. A., Wydzga, M. A., Fadde, J., & Sklar, L. (2010b). Mobilization of coarse surface layers in gravel-bedded rivers by finer gravel bed load. *Water Resources Research*, *46*, W07506. https://doi.org/10.1029/2009WR008329

Viparelli, E., Lauer, J. W., Belmont, P., & Parker, G. (2013). A numerical model to develop long-term sediment budgets using isotopic sediment fingerprints. *Computers & Geosciences*, *53*, 114–122. https://doi.org/10.1016/j.cageo.2011.10.003

Walder, J. S., & Driedger, C. L. (1993). *Volcano fact sheet; glacier-generated debris flows at Mount Rainier (No. 93–124)*. US Geological Survey.

Walder, J. S., & Driedger, C. L. (1994). Rapid geomorphic change caused by glacial outburst floods and debris flows along Tahoma Creek, Mount Rainier, Washington, USA. *Arctic and Alpine Research*, *26*(4), 319–327. https://doi.org/10.2307/1551792

Warrick, J. A., Bountry, J. A., East, A. E., Magirl, C. S., Randle, T. J., Gelfenbaum, G., et al. (2015). Large-scale dam removal on the Elwha River, Washington, USA: Source-to-sink sediment budget and synthesis. *Geomorphology*, *246*, 729–750. https://doi.org/10.1016/j.geomorph.2015.01.010

Welber, M., Papangelakis, E., Ashmore, P., & MacVicar, B. (2020). Experiments on restoring alluvial cover in straight and meandering rivers using gravel augmentation. *River Research and Applications*, *36*(8), 1543–1558. https://doi.org/10.1002/rra.3699

Wilcock, P. R., & Crowe, J. C. (2003). Surface-based transport model for mixed-size sediment. *Journal of Hydraulic Engineering*, *129*(2), 120–128. https://doi.org/10.1061/(ASCE)0733-9429(2003)129:2(120)

Wohl, E., & Scott, D. N. (2017). Wood and sediment storage and dynamics in river corridors. *Earth Surface Processes and Landforms*, *42*(1), 5–23. https://doi.org/10.1002/esp.3909

Wolman, M. G. (1954). A method of sampling coarse river-bed material. *Transactions, American Geophysical Union*, *35*(6), 951–956. https://doi.org/10.1029/tr035i006p00951

Wooster, J. K., Dusterhoff, S. R., Cui, Y., Sklar, L. S., Dietrich, W. E., & Malko, M. (2008). Sediment supply and relative size distribution effects on fine sediment infiltration into immobile gravels. *Water Resources Research*, *44*, W03424. https://doi.org/10.1029/2006WR005815

Reference From the Supporting Information

Pitlick, J., Cui, Y., & Wilcock, P. (2009). Manual for computing bed load transport using BAGS (Bedload Assessment for Gravel-bed Streams) Software. *General Technical Reports RMRS-GTR-223*,(p. 45). USDA Forest Service, Rocky Mountain Research Station. https://doi.org/10.2737/rmrs-gtr-223